

Superfluidity and non-monogamous pairing at unitarity

Dean Lee

Department of Physics, North Carolina State University, Raleigh, NC 27695

Abstract

We present lattice results for spin-1/2 fermions at unitarity, where the effective range of the interaction is zero and the scattering length is infinite. We measure the spatial coherence of difermion pairs for a system of 6, 10, 14, 18, 22, 26 particles with equal numbers of up and down spins in a periodic cube. Using Euclidean time projection, we analyze ground state properties and transient behavior due to low-energy excitations. The results indicate a low-energy excitation consistent with two quasiparticles moving in opposite directions at approximately 0.8 times the Fermi momentum. However the excitation lies well below twice the pairing gap estimated from even-odd ground state energy staggering and couples strongly to the difermion order parameter. In order to explain this we develop a theoretical framework for non-monogamous pairing and an interpretation of the two-quasiparticle excitation as two counterpropagating half rotons.

Contents

I. Introduction	2
II. O ₂ -diagonal long-range order	4
III. Measured observables in continuum notation	5
IV. Lattice formalism	6
V. Transfer matrix projection method	9
VI. Lattice parameters and error estimates	13
VII. Numerical crosschecks	14
VIII. Results for the renormalization constant	16
IX. Results for the t -dependent profile of G_2	19
X. Results for the lowest excitation energy	21
XI. Path integral permutations	26
XII. Rotons	33
XIII. Discussion	39
XIV. Summary	41
XV. Acknowledgements	41
References	41

I. INTRODUCTION

The unitary limit describes a many-body system of nonrelativistic spin-1/2 fermions with zero-range attraction and infinite scattering length. While the unitary limit has a well-defined continuum limit and strong interactions, at zero temperature it has no intrinsic

physical scale other than the interparticle spacing. This implies for example at zero temperature the energy per particle and pairing gap are both given by the Fermi energy times a dimensionless constant.

The universal nature of the unitary limit endows it relevance to several areas of physics and the subject has received much recent interest. The ground state is believed to be superfluid with properties somewhere between a Bardeen-Cooper-Schrieffer (BCS) fermionic superfluid at weak coupling and a Bose-Einstein condensate (BEC) of bound dimers at strong coupling [1, 2, 3]. In solid state physics it has been suggested that the crossover from BCS fermionic superfluid to BEC bosonic superfluid describes the pseudogap phase in high-temperature cuprate superconductors [4]. In atomic physics BCS-BEC crossover has been studied extensively with trapped ultracold ^6Li and ^{40}K atoms. The atoms are sufficiently far apart that the effective range of the interaction is negligible while the scattering length can be adjusted using a magnetic-field Feshbach resonance [5, 6, 7, 8]. In nuclear physics the unitary limit is relevant to the properties of cold dilute neutron matter. The neutron scattering length is about 18 fm while the effective range is 2.8 fm. Therefore the unitary limit is approximately realized when the interparticle spacing is about 5–10 fm, roughly 0.5%–5% of normal nuclear matter density. Superfluid neutrons at around this density may be present in the inner crust of neutron stars [9, 10].

In this study we measure the low-energy excitations of unpolarized spin-1/2 fermions in the unitary limit. We use the same lattice projection technique used in [11] to measure the ground state energy. We start with a quantum state with the desired quantum numbers and use the Euclidean time projection operator e^{-Ht} to filter out high-energy excitations. After this filtering we measure spatial correlations of the superfluid order parameter as a function of the projection time t . At asymptotically large values of t we see long-range order consistent with spontaneously broken $U(1)$ fermion-number symmetry and a superfluid ground state. At intermediate times we see exponential decay in the t -dependent signal and identify a low-energy excitation consistent with two quasiparticles moving in opposite directions at approximately 0.8 times the Fermi momentum. However the excitation lies well below twice the pairing gap estimated from even-odd staggering of the ground state energy and couples strongly to the dimer order parameter. This does not seem to fit into the usual picture of one-to-one pairing of fermions in the condensate and unpaired quasiparticles. We explore the possibility of non-monogamous pairing between opposite spin fermions and propose an

interpretation of the two-quasiparticle excitation as two counterpropagating half rotons.

II. OFF-DIAGONAL LONG-RANGE ORDER

Written in continuum notation the Hamiltonian for the unitary limit is

$$H = \frac{1}{2m} \int d^3x \sum_{i=\uparrow,\downarrow} \left[\sum_{\mathbf{r}} a_i^\dagger(\mathbf{r}) \tilde{r}^2 a_i(\mathbf{r}) + C \sum_{\mathbf{r}} a_\uparrow^\dagger(\mathbf{r}) a_\downarrow^\dagger(\mathbf{r}) a_\uparrow(\mathbf{r}) a_\downarrow(\mathbf{r}) \right] \quad (1)$$

a_i and a_i^\dagger are annihilation and creation operators for fermions with spin i . The mass of the fermion is m , and the coefficient C is cutoff dependent. We discuss later how in lattice regularization C is tuned to make the s -wave scattering length infinite.

The unitary limit Hamiltonian has a global $U(1)$ fermion-number symmetry

$$\begin{pmatrix} a_\uparrow(\mathbf{r}) \\ a_\downarrow(\mathbf{r}) \end{pmatrix} \rightarrow e^{i\theta} \begin{pmatrix} a_\uparrow(\mathbf{r}) \\ a_\downarrow(\mathbf{r}) \end{pmatrix}; \quad (2)$$

where θ is any real constant. It also has a global $SU(2)$ spin symmetry

$$\begin{pmatrix} a_\uparrow(\mathbf{r}) \\ a_\downarrow(\mathbf{r}) \end{pmatrix} \rightarrow e^{i\vec{\theta} \cdot \vec{\tau}} \begin{pmatrix} a_\uparrow(\mathbf{r}) \\ a_\downarrow(\mathbf{r}) \end{pmatrix}; \quad (3)$$

where $\vec{\tau}$ denotes the 2×2 Pauli spin matrices and $\vec{\theta}$ is any real constant three-component vector. Since there is no coupling between intrinsic spin and orbital angular momentum, this $SU(2)$ symmetry should be regarded as an internal symmetry decoupled from spatial rotations.

The lowest-dimensional local bosonic operator that can be constructed from the annihilation field operators is

$$\phi^2(\mathbf{r}) = a_\uparrow(\mathbf{r}) a_\downarrow(\mathbf{r}); \quad (4)$$

We note that ϕ^2 is invariant under the $SU(2)$ spin symmetry but phase rotates under the $U(1)$ fermion-number symmetry,

$$\phi^2(\mathbf{r}) \rightarrow e^{2i\theta} \phi^2(\mathbf{r}); \quad (5)$$

Therefore if there is some critical temperature below which ϕ^2 has long-range spatial correlations,

$$\lim_{|\mathbf{r}'| \rightarrow \infty} \langle \phi^2(\mathbf{r}) \phi^2(\mathbf{r}') \rangle \neq 0; \quad (6)$$

then the $U(1)$ fermion-number symmetry is spontaneously broken. While there are many different ways to characterize superfluid behavior, this condition of off-diagonal long-range order [12, 13] is usually regarded as the standard definition for superfluidity.

III. MEASURED OBSERVABLES IN CONTINUUM NOTATION

In order to highlight the physics content of the lattice calculation we summarize the measured observables in continuum notation. We refer to a state with N_\uparrow up-spin fermions and N_\downarrow down-spin fermions as an $N_\uparrow; N_\downarrow$ state. We also specify the total momentum P and total spin S of the $SU(2)$ spin representation. Let $|\psi_0^{\text{free}}\rangle$ be the free Fermi ground state for the $N_\uparrow; N_\downarrow$ system with $P = 0$ and $S = 0$. We filter out high-energy states using the Euclidean-time projection operator e^{-Ht} ,

$$|j(t)\rangle = e^{-Ht} |\psi_0^{\text{free}}\rangle \quad (7)$$

With the projected states $|j(t)\rangle$ we measure the correlation function $G_2(\mathbf{x}; t_1; t_2)$,

$$G_2(\mathbf{x}; t_1; t_2) = \frac{1}{h} \frac{\langle j(t_1) | j^{2y}(\mathbf{x}) | j(t_2) \rangle}{\langle j(t_1) | j(t_2) \rangle}, \quad (8)$$

where h is a renormalization coefficient set by the condition

$$\lim_{t_1, t_2 \rightarrow 1} G_2(0; t_1; t_2) = 1. \quad (9)$$

For large t we have the asymptotic form

$$|j(t)\rangle = c_0 e^{E_0 t} |j_0\rangle + c_1 e^{E_1 t} |j_1\rangle + \dots \quad (10)$$

$|j_0\rangle$ is the normalized ground state with energy E_0 , and $|j_1\rangle$ is the normalized first excited state with energy E_1 . We anticipate the possibility of degeneracy in the low-energy spectrum corresponding with two-particle excitations with momenta \mathbf{k} and \mathbf{k} . Since we use a periodic cube with lattice regularization, quantum states in the same irreducible representation of the cubic lattice symmetry group $SO(3; Z)$ are exactly degenerate in energy. But there might also be approximately degenerate excited states whose energy differences are not adequately resolved by the finite values of t measured. We use the notation $|j_{1,i}\rangle$ for the complete set of normalized degenerate excited states with energy E_1 . Using the asymptotic form (10) we get

$$G_2(\mathbf{x}; t_1; t_2) = A_{00}(\mathbf{x}) + A_{01}(\mathbf{x}) e^{(E_1 - E_0)t_2} + A_{10}(\mathbf{x}) e^{(E_1 - E_0)t_1} + A_{11}(\mathbf{x}) e^{(E_1 - E_0)(t_1 + t_2)} + \dots \quad (11)$$

where

$$A_{00}(\mathbf{x}) = \frac{1}{h} \langle j_0 | j^{2y}(\mathbf{x}) | j_0 \rangle \quad (12)$$

$$A_{01}(\mathbf{x}) = \frac{1}{i} \sum_j \frac{c_0 c_{1,ji}}{\dot{J}_0^2} h_{0j}^{2y(\mathbf{x})} \mathcal{J}^2(\mathbb{0}) j_{1,ji}; \quad (13)$$

$$A_{10}(\mathbf{x}) = \frac{1}{i} \sum_j \frac{c_{1,ji} c_0}{\dot{J}_0^2} h_{1,ji}^{2y(\mathbf{x})} \mathcal{J}^2(\mathbb{0}) j_{0i}; \quad (14)$$

$$A_{11}(\mathbf{x}) = \frac{1}{i} \sum_{ji^0} \frac{c_{1,ji} c_{1,ji^0}}{\dot{J}_0^2} h_{1,ji}^{2y(\mathbf{x})} \mathcal{J}^2(\mathbb{0}) j_{1,ji^0} - \frac{1}{i} \sum_j \frac{\dot{J}_{1,ji}^2}{\dot{J}_0^2} h_{0j}^{2y(\mathbf{x})} \mathcal{J}^2(\mathbb{0}) j_{0i}; \quad (15)$$

From the definition of it follows that $A_{00}(\mathbb{0}) = 1$. In order to determine whether the strongest transient signal comes from $A_{01}(\mathbf{x})$ and $A_{10}(\mathbf{x})$ or $A_{11}(\mathbf{x})$ we will calculate $G^2(\mathbf{x}; t_1; t_2)$ for two different large time combinations. In one case we let $t_1 = t_2$ and send both to infinity. In the other case we let t_2 be large but fixed and take the limit as t_1 goes to infinity. By analyzing the time dependence we extract the energy difference $E_1 - E_0$, and from the spatial dependence we measure the momentum of the particles in $j_{1,ji}$ which couple to $^{2y}(\mathbf{x}) \mathcal{J}^2(\mathbb{0})$.

IV. LATTICE FORMALISM

Throughout our discussion of the lattice calculation we use dimensionless parameters and operators which correspond with physical values multiplied by the appropriate power of the spatial lattice spacing a . When we need to specify quantities in physical units we write the subscript 'phys'. In our notation the four-component integer vector \mathbf{n} labels the lattice sites of a $3+1$ dimensional lattice with dimensions $L^3 \times L_t$. \mathbf{n}_s gives the spatial part of \mathbf{n} , while n_t is the time component. We write $\hat{\mathbf{l}}_s = \hat{1}, \hat{2}, \hat{3}$ for the spatial lattice unit vectors and $\hat{0}$ for the temporal lattice unit vector. The temporal lattice spacing is given by a_t , and $\tau = a_t/a$ is the ratio of the temporal to spatial lattice spacing. We also define $h = \tau = (2m)$, where m is the fermion mass in lattice units.

We briefly discuss four different lattice formulations: the transfer matrix formalism with and without auxiliary fields, and the path integral formalism with and without auxiliary fields. While in the main calculation we use only the transfer matrix formalism with auxiliary fields, the other formulations are useful to provide numerical checks of the simulation data. The four formulations agree exactly even for nonzero spatial and temporal lattice spacings.

The first formulation we consider is the path integral formalism with auxiliary fields. This has been used in varying forms in several grand canonical mean field calculations and lattice simulations at nonzero temperature [14, 15, 16, 17, 18, 19, 20]. We let $c_i(\mathbf{r})$ and $c_{\bar{i}}(\mathbf{r})$ be anticommuting Grassmann fields for spin i , and $s(\mathbf{r})$ be an auxiliary Hubbard-Stratonovich field. Let Z be the partition function

$$Z = \int \mathcal{D}s \mathcal{D}c \mathcal{D}c_{\bar{i}} \exp [S(s; c; c_{\bar{i}})]; \quad (16)$$

where

$$\mathcal{D}s = \prod_{\mathbf{r}} ds(\mathbf{r}); \quad (17)$$

$$\mathcal{D}c \mathcal{D}c_{\bar{i}} = \prod_{\mathbf{r}; i} dc_i(\mathbf{r}) dc_{\bar{i}}(\mathbf{r}); \quad (18)$$

We take as our standard lattice path integral action

$$S(s; c; c_{\bar{i}}) = \sum_{\mathbf{r}; i} \sum_{\mathbf{r}'} h_{\mathbf{r}\mathbf{r}'} c_i(\mathbf{r}) c_{\bar{i}}(\mathbf{r} + \hat{\mathbf{o}}) e^{i \frac{p}{c} \tau s(\mathbf{r}) + \frac{c}{2} \tau} (1 - 6h) c_i(\mathbf{r}) c_{\bar{i}}(\mathbf{r}) + \sum_{\mathbf{r}; i} \sum_{\mathbf{r}'} h_{\mathbf{r}\mathbf{r}'} c_i(\mathbf{r}) c_{\bar{i}}(\mathbf{r} + \hat{\mathbf{s}}) + c_i(\mathbf{r}) c_{\bar{i}}(\mathbf{r} - \hat{\mathbf{s}}) + \frac{1}{2} \sum_{\mathbf{r}} [s(\mathbf{r})]^2; \quad (19)$$

If we include a chemical potential then the action becomes

$$S(s; c; c_{\bar{i}}) = \sum_{\mathbf{r}; i} \sum_{\mathbf{r}'} h_{\mathbf{r}\mathbf{r}'} c_i(\mathbf{r}) c_{\bar{i}}(\mathbf{r} + \hat{\mathbf{o}}) e^{i \frac{p}{c} \tau s(\mathbf{r}) + \frac{c}{2} \tau} e^{-\tau} (1 - 6h) c_i(\mathbf{r}) c_{\bar{i}}(\mathbf{r}) + \sum_{\mathbf{r}; i} \sum_{\mathbf{r}'} h_{\mathbf{r}\mathbf{r}'} c_i(\mathbf{r}) c_{\bar{i}}(\mathbf{r} + \hat{\mathbf{s}}) + c_i(\mathbf{r}) c_{\bar{i}}(\mathbf{r} - \hat{\mathbf{s}}) + \frac{1}{2} \sum_{\mathbf{r}} [s(\mathbf{r})]^2; \quad (20)$$

From this point on it is easy to follow how the chemical potential enters into the other formulations. Therefore we simplify the discussion by setting the chemical potential to zero.

In order to connect the path integral with the transfer matrix formalism, we use the correspondence [21, 22]

$$\begin{aligned} \text{Tr} & : F_{L_t}^Y : a_{i^0}^Y(\mathbf{r}_S^0); a_i(\mathbf{r}_S) : & : F_{i^0}^Y(\mathbf{r}_S^0); a_i(\mathbf{r}_S) : \\ & & = \\ & = \int \mathcal{D}c \mathcal{D}c_{\bar{i}} \exp : \prod_{n_t=0}^{L_t-1} \prod_{\mathbf{r}; i} c_i(\mathbf{r}_S; n_t) [c_i(\mathbf{r}_S; n_t) - c_i(\mathbf{r}_S; n_t + 1)] : \\ & & = \prod_{n_t=0}^{L_t-1} F_{n_t} [c_{i^0}^Y(\mathbf{r}_S^0; n_t); c_i(\mathbf{r}_S; n_t)] \end{aligned} \quad (21)$$

where $c_i(\mathbf{r}_s; L_t) = c_i(\mathbf{r}_s; 0)$: We use $a_i(\mathbf{r}_s)$ and $a_i^y(\mathbf{r}_s)$ to denote the fermion annihilation and creation operators respectively for spin i . The $:$ symbols in the top line of (21) indicate normal ordering. Let us define the transfer matrix operator

$$M_{n_t}(s) = \exp \left\langle \prod_{n_s; i} \left[e^{-\frac{h}{c} \tau S(\mathbf{r}_s; n_t) + \frac{c-t}{2} (1-6h) \prod_i a_i^y(\mathbf{r}_s) a_i(\mathbf{r}_s)} + h \prod_{n_s; i; j} a_i^y(\mathbf{r}_s) a_i(\mathbf{r}_s + \hat{s}) + a_i^y(\mathbf{r}_s) a_i(\mathbf{r}_s - \hat{s}) \right] \right\rangle ; \quad (22)$$

We can write the partition function as

$$Z / \text{D s Tr fM}_{L_t-1}(s) = \int \mathcal{D}(\mathbf{s}) \exp \left[\frac{1}{2} \sum_n [\mathbf{s}(\mathbf{n})]^2 \right] ; \quad (23)$$

We now remove the auxiliary field. Integrating over $\mathbf{s}(\mathbf{n})$ in the path integral we obtain [23]

$$Z / \text{D c d c} \exp [S(c; c)] ; \quad (24)$$

$$S(c; c) = \sum_n c_i(\mathbf{n}) c_i(\mathbf{n} + \hat{0}) (1-6h) c_i(\mathbf{n}) c_i(\mathbf{n}) + h \prod_{n; i; j} c_i(\mathbf{n}) c_i(\mathbf{n} + \hat{s}) + c_i(\mathbf{n}) c_i(\mathbf{n} - \hat{s}) e^{c-t} (1-6h)^2 \prod_n c_{\#}(\mathbf{n}) c_{\#}(\mathbf{n}) c_{\#}(\mathbf{n}) c_{\#}(\mathbf{n}) ; \quad (25)$$

This is probably the simplest formulation for computing Feynman diagrams and the most convenient for setting the lattice interaction coefficient C . As shown in [15] the procedure for setting C involves summing the bubble diagrams shown in FIG. 1, locating the pole in the scattering amplitude, and comparing with Luscher's formula for energy levels in a finite periodic cube [24, 25],

$$E_{\text{pole}} = \frac{4 a_{\text{scatt}}}{m L^3} \left[1 - c_1 \frac{a_{\text{scatt}}}{L} + c_2 \frac{a_{\text{scatt}}^2}{L^2} + \dots \right] ; \quad (26)$$

where $c_1 = 2.837297$; $c_2 = 6.375183$. Taking the limit $a_{\text{scatt}} \rightarrow 1$ we get the interaction coefficient for the unitary limit.

We can use (21) again to derive the corresponding transfer matrix formalism without auxiliary fields,

$$Z / \text{Tr fM}_{L_t-1} = \int \mathcal{D}(\mathbf{c}) ; \quad (27)$$

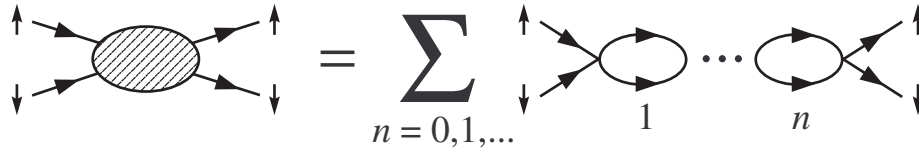


FIG . 1: Two-particle scattering bubble chain diagrams

where

$$M_{n_t} = \exp \left[\sum_{\mathbf{n}_s} \left(6h \sum_{i,j} a_i^y(\mathbf{n}_s) a_j(\mathbf{n}_s) + h \sum_{i,j} a_i^y(\mathbf{n}_s) a_j(\mathbf{n}_s + \hat{e}_s) + a_i^y(\mathbf{n}_s) a_j(\mathbf{n}_s - \hat{e}_s) \right) \right] \quad (28)$$

Since there is no time-dependent auxiliary field, M_{n_t} is the same for each time step n_t . This formulation is useful in few-body systems with no sign problem. In [23] it was used to calculate the binding energy of the SU(4) Wigner-symmetric triton.

V. TRANSFER MATRIX PROJECTION METHOD

We use the transfer matrix projection method introduced in [11]. In this paper we consider the values $N = 1;3;5;7;9;11;13$. For each spin we list the momentum states comprising χ_0^{free} in the order shown in Table 1. We observe that for each value of N , χ_0^{free} has zero total momentum and zero total spin. For $N = 7$ we have the special case where χ_0^{free} is also invariant under SO(3;Z) rotations.

N	additional momentum states
1	$h0;0;0i$
3	$\frac{2}{L};0;0 ; \frac{2}{L};0;0$
5	$0;\frac{2}{L};0 ; 0;\frac{2}{L};0$
7	$0;0;\frac{2}{L} ; 0;0;\frac{2}{L}$
9	$\frac{2}{L};\frac{2}{L};0 ; \frac{2}{L};\frac{2}{L};0$
11	$\frac{2}{L};\frac{2}{L};0 ; \frac{2}{L};\frac{2}{L};0$
13	$0;\frac{2}{L};\frac{2}{L} ; 0;\frac{2}{L};\frac{2}{L}$

Table 1. Filling sequence of momentum states

Using the auxiliary field transfer matrix defined in (22) we construct

$$j(t); si \quad M_{n_t-1}(s) \quad \text{free} \quad ; \quad (29)$$

where $t = n_t a_t$. This is the analog of

$$j(t)i = e^{H t} \quad \text{free} \quad (30)$$

defined above in the continuum notation. We compute spatial correlations of the difermion pair operator $\psi^2(\mathbf{r}_s) = a^\dagger(\mathbf{r}_s) a(\mathbf{r}_s)$,

$$G_{\psi^2}^{\text{bare}}(\mathbf{r}_s; t_1; t_2) = \frac{\int \mathcal{D}s \, h(t_1); sj^{2y}(\mathbf{r}_s) \psi^2(0) j(t_2); si \exp\left[-\frac{1}{2} \int \mathcal{D}\mathbf{r} [s(\mathbf{r})]^2\right]}{\int \mathcal{D}s \, h(t_1); sj(t_2); si \exp\left[-\frac{1}{2} \int \mathcal{D}\mathbf{r} [s(\mathbf{r})]^2\right]} : \quad (31)$$

The inner products in the numerator and denominator are to be defined shortly. We use the superscript 'bare' since matrix elements of the composite operators ψ^2 and ψ^{2y} diverge in the continuum limit. We take care of this renormalization by rescaling the correlation function,

$$G_{\psi^2}(\mathbf{r}_s; t_1; t_2) = \frac{1}{Z} G_{\psi^2}^{\text{bare}}(\mathbf{r}_s; t_1; t_2); \quad (32)$$

where

$$= \lim_{t_1, t_2 \rightarrow 1} G_{\psi^2}^{\text{bare}}(0; t_1; t_2); \quad (33)$$

$M_{n_t}(s)$ consists entirely of single-body operators interacting with the background auxiliary field and has no direct interactions between particles. This may not be obvious from the complicated form for $M_{n_t}(s)$ in (22). To see this more clearly we pretend for the moment that the N up-spin particles and N down-spin particles are all distinguishable. We label the newly distinguishable particles with the label $X = 1; 2; \dots; 2N - 1; 2N$: This error in quantum statistics has no effect on the final answer if the initial and final state wavefunctions are completely antisymmetric in the up-spin and down-spin variables. Since we have exactly one particle of each type X , the normal-ordered operator $M_{n_t}(s)$ can be factorized as a product of terms of the form

$$M_{n_t}(s) = \prod_X M_{n_t}^X(s); \quad (34)$$

where

$$M_{n_t}^X(s) = 1 + \frac{h}{c} e^{-\frac{p}{c} s(n_s, n_t) + \frac{c-t}{2}} (1 - 6h) \frac{iX}{1} a_X^y(n_s) a_X(n_s) + h \sum_{n_s; \hat{l}_s} a_X^y(n_s) a_X(n_s + \hat{l}_s) + a_X^y(n_s) a_X(n_s - \hat{l}_s) : \quad (35)$$

If the particle stays at the same spatial lattice site from time step n_t to $n_t + 1$, then the corresponding matrix element of $M_{n_t}^X(s)$ is

$$e^{-\frac{p}{c} s(n) + \frac{c-t}{2}} (1 - 6h) : \quad (36)$$

If the particle hops to a neighboring lattice site from time step n_t to $n_t + 1$ then the corresponding matrix element of $M_{n_t}^X(s)$ is h . All other elements of $M_{n_t}^X(s)$ are zero.

We can therefore compute the full $2N$ -body matrix element as the square of the determinant of the single-particle matrix elements,

$$\langle \text{free}_0 | M_{L_t-1}(s) | \text{free}_0 \rangle = [\det M(s; t_1 + t_2)]^2 ; \quad (37)$$

$$M_{ij}(s; t_1 + t_2) = \langle p_i | M_{L_t-1}^X(s) | p_j \rangle ; \quad (38)$$

where i, j go from 1 to N and $t_1 + t_2 = L_t a_t$. The states $|p_j\rangle$ are the single-particle momentum states for the up spins (or down spins) comprising our Slater determinant initial and final state $|\text{free}_0\rangle$. The square of the determinant arises from the fact that we have the same transfer matrix elements and the same momentum states $|p_j\rangle$ for both up and down spins. Since the square of the determinant is nonnegative, there is no sign problem.

We sample configurations according to the weight

$$\exp \left(-\frac{1}{2} \sum_n^X [s(n)]^2 + 2 \ln [\det M(s; t_1 + t_2)] \right) : \quad (39)$$

The updating procedure is done using hybrid Monte Carlo [26]. This involves computing molecular dynamics trajectories for

$$H(s; p) = \frac{1}{2} \sum_n^X (p(n))^2 + V(s); \quad (40)$$

where $p(\mathfrak{n})$ is the conjugate momentum for $s(\mathfrak{n})$ and

$$V(s) = \frac{1}{2} \sum_{\mathfrak{n}} (s(\mathfrak{n}))^2 - 2 \ln [\det M(s; t_1 + t_2)] : \quad (41)$$

More details of the updating procedure are given in [11]. For each configuration we compute the observable

$$O(\mathfrak{n}_s; t_1; t_2; s) = \frac{h(t_1; s; j^{2y(\mathfrak{n}_s)} \mathbb{0}) j(t_2; s; i)}{h(t_1; s; j(t_2); s; i)} : \quad (42)$$

This can be written in terms of the matrix $M(s; t_1 + t_2)$ as we now show.

We start with

$$h(t_1; s; j^{2y(\mathfrak{n}_s)} \mathbb{0}) j(t_2; s; i) = \int_0^{\text{free}} M_{L_t-1}(s) \int_{n_{t_2}} M(s) j^{2y(\mathfrak{n}_s)} \mathbb{0} M_{n_{t_2}-1}(s) \int_0^{\text{free}} M(s) j(i) : \quad (43)$$

where $t_1 + t_2 = L_t a_t$ and $t_2 = n_{t_2} a_t$. For each spin in the $j^{2y(\mathfrak{n}_s)} \mathbb{0}$ operator replaces one matrix element from $M(s; t_1 + t_2)$, call it the entry in the k th row and l th column, with the new matrix element

$$g_{kl}(\mathfrak{n}_s; s; t_1; t_2) = \int_{n_{t_2}} M_{L_t-1}(s) \int_{n_{t_2}} M(s) a_x^y(\mathfrak{n}_s) a_x \mathbb{0} M_{n_{t_2}-1}(s) \int_0^{\text{free}} M(s) j(i) : \quad (44)$$

Instead of the full $N \times N$ matrix determinant $\det M(s; t_1 + t_2)$, in this case we get $g_{kl}(\mathfrak{n}_s; s; t_1; t_2)$ times the entry in the k th row and l th column of the cofactor matrix of $M(s; t_1 + t_2)$. This cofactor matrix element is $(-1)^{k+l}$ times the determinant of the remaining $(N-1) \times (N-1)$ matrix with the k th row and l th column of $M(s; t_1 + t_2)$ deleted, and it can be calculated as

$$\det M(s; t_1 + t_2) M^{-1}(s; t_1 + t_2)_{lk} ; \quad (45)$$

where M^{-1} is the matrix inverse of M . Summing over k and l and squaring the result for the two spins, we get

$$\begin{aligned} & h(t_1; s; j^{2y(\mathfrak{n}_s)} \mathbb{0}) j(t_2; s; i) \\ & \left(\int_{n_{t_2}} M_{L_t-1}(s) \int_{n_{t_2}} M(s) j^{2y(\mathfrak{n}_s)} \mathbb{0} M_{n_{t_2}-1}(s) \int_0^{\text{free}} M(s) j(i) \right)^2 \\ & = \det M(s; t_1 + t_2) \sum_{k,l} g_{kl}(\mathfrak{n}_s; s; t_1; t_2) M^{-1}(s; t_1 + t_2)_{lk} : \quad (46) \end{aligned}$$

Therefore our observable is

$$O(\mathfrak{n}_s; t_1; t_2; s) = \left(\int_{n_{t_2}} M_{L_t-1}(s) \int_{n_{t_2}} M(s) j^{2y(\mathfrak{n}_s)} \mathbb{0} M_{n_{t_2}-1}(s) \int_0^{\text{free}} M(s) j(i) \right)^2 \sum_{k,l} g_{kl}(\mathfrak{n}_s; s; t_1; t_2) M^{-1}(s; t_1 + t_2)_{lk} : \quad (47)$$

By measuring the ensemble average of $O(\mathfrak{n}_s; t_1; t_2; s)$ we get an unbiased estimate of $G_2^{\text{bare}}(\mathfrak{n}_s; t_1; t_2)$:

VI. LATTICE PARAMETERS AND ERROR ESTIMATES

Our choice for the physical values of the fermion mass and lattice spacings are irrelevant to the universal physics of the unitary limit. Nevertheless we must assign values to these parameters, and the values we choose are motivated by the dilute neutron system. We use a fermion mass of 939 MeV and lattice spacings $a = (50 \text{ MeV})^{-1}$, $a_t = (24 \text{ MeV})^{-1}$. For these parameters we find in the unitary limit, $C_{\text{phys}} = 1.203 \cdot 10^4 \text{ MeV}^2$.

For each simulation we compute roughly $2 \cdot 10^5$ hybrid Monte Carlo trajectories, split across four processors running completely independent trajectories. Averages and errors are computed by comparing the results of each processor. We use double precision arithmetic to compute $\det M(s; t_1 + t_2)$ and $O(\mathfrak{n}_s; t_1; t_2; s)$. All systematic errors produced by double precision round-off error and exceptional configurations are monitored in the following way. We introduce a small positive parameter ϵ and reject any hybrid Monte Carlo trajectories which generate a configuration with

$$|\det M(s; t_1 + t_2)| < \prod_{i=1; \dots; N}^Y |M_{ii}(s; t_1 + t_2)|. \quad (48)$$

We then take the limit $\epsilon \rightarrow 0$ to determine if poorly-conditioned matrices make any detectable contribution to our observables. We consider values for ϵ as small as 10^7 . If as we take $\epsilon \rightarrow 0$ any systematic error can be detected above the stochastic error level, then we throw out the measurement and do not include it in the final results. The error bars we present are therefore estimates of the total error for each lattice system. There are no additional errors other than the lattice spacing dependence.

In the unitary limit our Euclidean variables t_1 and t_2 can be replaced by the dimensionless combinations $\frac{t_1}{m L^2}$ and $\frac{t_2}{m L^2}$. More convenient though is to use the dimensionless combinations $E_F t_1$ and $E_F t_2$, where E_F is the Fermi energy

$$E_F = \frac{k_F^2}{2m} \approx 7.596 \frac{N^{2/3}}{m L^2}. \quad (49)$$

At unitarity we can reach the continuum limit at fixed particle number by increasing L , the length of the periodic cube in lattice units. This may seem an unusual way to take

the continuum limit. It works only in scale invariant theories such as the unitary limit or noninteracting fermions where the only physical scale is the interparticle spacing. Since the number of particles is fixed, the spacing between particles as measured in lattice units increases as we increase L . Therefore $L \rightarrow \infty$ corresponds with the continuum limit. By comparing results for different L we obtain an error estimate for the extrapolation to the continuum limit.

VII. NUMERICAL CROSSCHECKS

To test the lattice codes, we have run simulations for several systems where the final answer can be calculated accurately by alternative means. For the first test we consider the noninteracting fermion system for the $7;7$ system with total momentum $P = 0$ and total spin $S = 0$. We take $L = 4$ and set L_t large enough to extract the limit

$$\lim_{t_1, t_2 \rightarrow \infty} G_2^{\text{bare}}(\mathbf{n}_s; t_1; t_2) \quad (50)$$

for $\mathbf{n}_s = (n_x; 0; 0)$ with $n_x = 0; 1; 2$. We perform the numerical check using the path integral action $S(c; c)$ in (25). For temperature $T = 0.022E_F$ and chemical potential $\mu = 0.97E_F$ we apply the free field Feynman rules for the G_2 correlation function. For this chemical potential at such low temperatures we should see 7 up spins and 7 down spins in the ground state with $P = 0$ and $S = 0$. A comparison of the simulation results and the free grand canonical calculations is shown Table 2. We see that the free fermion results agree to six-digit precision.

n_x	Simulation results	Free grand canonical
0	$1.19629 \cdot 10^{-2}$	$1.19629 \cdot 10^{-2}$
1	$6.10352 \cdot 10^{-3}$	$6.10352 \cdot 10^{-3}$
2	$2.19727 \cdot 10^{-3}$	$2.19727 \cdot 10^{-3}$

Table 2. Simulation results and free grand canonical calculations for $7;7$

Next we turn on a weak attractive coupling $C_{\text{phys}} = 1.25 \cdot 10^5 \text{ MeV}^{-2}$ for the same $7;7$ system with $P = 0$ and $S = 0$. This coupling corresponds with a weak-coupling low-density expansion parameter $k_F a_{\text{scatt}} = 0.043$. Using $T = 0.022E_F$ and $\mu = 0.97E_F$ we use the

path integral action $S(c;c)$ to compute the free fermion result as well as the $O(k_F a_{\text{scatt}})$ correction to the 2 correlation function. The $O(k_F a_{\text{scatt}})$ term requires summing the two-particle bubble chain shown in FIG. 1. A comparison of the simulation results and perturbative calculations is shown in Table 3. The $O(k_F^2 a_{\text{scatt}}^2)$ correction should be of size roughly 10^{-4} for $n_x = 0$, $5 \cdot 10^{-5}$ for $n_x = 1$; and $2 \cdot 10^{-5}$ for $n_x = 2$. We see that the simulation results and perturbative calculations agree within deviations roughly matching the size estimates for the $O(k_F^2 a_{\text{scatt}}^2)$ term.

n_x	Simulation results	Perturbative grand canonical
0	1.3715(1) 10^{-2}	1.3775 10^{-2}
1	6.999(2) 10^{-3}	7.0295 10^{-3}
2	2.536(1) 10^{-3}	2.5476 10^{-3}

Table 3. Simulation results and perturbative grand canonical calculations for 7;7

To test that the code is running properly at the unitary limit, we perform simulations for the 1;1 system at $P = 0$ and $S = 0$ at unitarity. We use $L = 4$ and compute $G_2^{\text{bare}}(n_s; t_1; t_2)$. We take $n_s = (n_x; 0; 0)$ for $n_x = 0; 1; 2$ and various numbers of time steps $n_{t_1} = n_{t_2}$. Since there are only two particles with zero total momentum there should be no dependence on the spatial coordinate n_x . For the numerical check we use M_{n_t} , the transfer matrix without auxiliary fields defined in (28), to compute the exact two-body transfer matrix in the rest frame. The results for the lattice simulation and the exact two-body calculation are shown in Table 4. We see that the simulation results agree with the exact results up to errors the size of the estimated stochastic noise.

n_x	$n_{t_1} = n_{t_2} = 2$	$n_{t_1} = n_{t_2} = 4$	$n_{t_1} = n_{t_2} = 6$
0	6.946(9) 10^{-4}	1.156(4) 10^{-3}	1.564(4) 10^{-3}
1	6.88(3) 10^{-4}	1.19(4) 10^{-3}	1.58(6) 10^{-3}
2	6.92(1) 10^{-4}	1.147(6) 10^{-3}	1.53(3) 10^{-3}
Exact	6.948 10^{-4}	1.153 10^{-3}	1.573 10^{-3}

Table 4: Simulation results and exact two-body calculation for 1;1 at unitarity

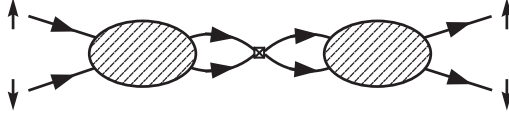


FIG. 2: One insertion of the operator $a_{\#}^{\dagger}(\mathbf{x})a_{\#}(\mathbf{x})a_{\#}(\mathbf{x})a_{\#}^{\dagger}(\mathbf{x})$

VIII. RESULTS FOR THE RENORMALIZATION CONSTANT

Throughout we consider systems with total momentum $P = 0$ and total spin $S = 0$. The renormalization constant for the $N;N$ system is given by

$$= \lim_{t_1, t_2 \rightarrow 1} G_{\frac{1}{2}}^{\text{bare}}(0; t_1; t_2) = \langle 0 | j a_{\#}^{\dagger}(0) a_{\#}^{\dagger}(0) a_{\#}(0) a_{\#}(0) | j_0 \rangle \quad (51)$$

where $|j_0\rangle$ is the normalized ground state. As shown in FIG. 2, one insertion of the operator $a_{\#}^{\dagger}(\mathbf{x})a_{\#}^{\dagger}(\mathbf{x})a_{\#}(\mathbf{x})a_{\#}(\mathbf{x})$ produces two extra fermion bubbles. In the continuum limit each of these bubbles are proportional to the inverse lattice spacing a^{-1} plus momentum-dependent terms which are finite as $a \rightarrow 0$. Therefore in the continuum limit χ_{phys} is proportional to a^{-2} plus subleading terms proportional to a^{-1} .

The coefficient of a^{-2} in χ_{phys} contains some useful information about physics near the unitarity point. We note that

$$= \langle 0 | j a_{\#}^{\dagger}(0) a_{\#}^{\dagger}(0) a_{\#}(0) a_{\#}(0) | j_0 \rangle = \frac{1}{tL^3} \frac{d}{dC^0} \langle 0 | j M_{nt} | j_0 \rangle; \quad (52)$$

where M_{nt} is the transfer matrix without auxiliary fields defined in (28), and

$$C^0 = \frac{e^{C^0 t} - 1}{t} (1 - 6h)^2; \quad (53)$$

We have dropped terms which are $O(a_t)$ and vanish as the temporal lattice spacing goes to zero. If E_0 is the ground state energy then

$$\langle 0 | j M_{nt} | j_0 \rangle = e^{E_0 t}; \quad (54)$$

$$\frac{1}{tL^3} \frac{d}{dC^0} e^{E_0 t} = \frac{1}{L^3} \frac{dE_0}{dC^0}; \quad (55)$$

Let us parameterize the ground state energy per particle near the unitary limit as an expansion in $k_F^{-1} a_{\text{scatt}}^1$,

$$\frac{E_0}{N + N} = \frac{3 k_F^2}{5 2m} \left(k_F^{-1} a_{\text{scatt}}^1 + O(k_F^{-2} a_{\text{scatt}}^2) \right) : \quad (56)$$

The renormalization condition relating C^0 and a_{scatt} gives [15]

$$\frac{d}{da_{\text{scatt}}^1} = \frac{m}{4} \frac{d}{dC^0} = \frac{m C^0}{4} \frac{d}{dC^0} : \quad (57)$$

Using

$$k_F = \frac{(6^{-2} N)^{1/3}}{L} ; \quad (58)$$

and combining (55), (56), (57) we find

$$\frac{d}{da_{\text{scatt}}^1} = \frac{5m}{3N k_F} \frac{dE_0}{da_{\text{scatt}}^1} = \frac{5m^2 C^0 L^4}{12 (6^{-2})^{1/3} N^{4/3}} : \quad (59)$$

Since C_{phys}^0 is proportional to the lattice spacing a , we deduce that the leading divergence of ϵ_{phys} is proportional to a^2 as predicted before. This anomalous dimensional scaling can also be seen from the L^4 dependence of ϵ_{phys} rather than the naive L^6 scaling expected for an operator which is the square of a local density.

We determine ϵ_{phys} by fitting $G_2^{\text{bare}}(0; t=2; t=2)$ at large $E_F t$ to the asymptotic form

$$G_2^{\text{bare}}(0; t=2; t=2) \sim \frac{1}{E_F t} . \quad (60)$$

The value of ϵ_{phys} is then used to determine ϵ_1 . We show the results for $N = 3;5;7;9;11;13$ and $L = 4;5;6$ in Table 5. We have extrapolated linearly in L^{-1} as $L \rightarrow \infty$ to remove the subleading a^1 dependence in $G_2^{\text{bare}}(0; t=2; t=2)$. If there are no significant changes for $N > 13$ we estimate that in the limit $N \rightarrow \infty$, $\epsilon_1 = 1.0(1)$:

L	3;3	5;5	7;7	9;9	11;11	13;13
4	0:696 (2)	0:647 (2)	0:597 (2)	0:595 (2)		
5	0:77 (1)	0:719 (5)	0:662 (3)	0:661 (2)	0:652 (2)	0:639 (2)
6	0:84 (3)	0:785 (4)	0:69 (1)	0:711 (4)	0:71 (1)	0:70 (1)
1	1:08 (4)	1:05 (4)	0:91 (4)	0:93 (4)	1:00 (5)	1:01 (5)

Table 5: Results for ϵ_1

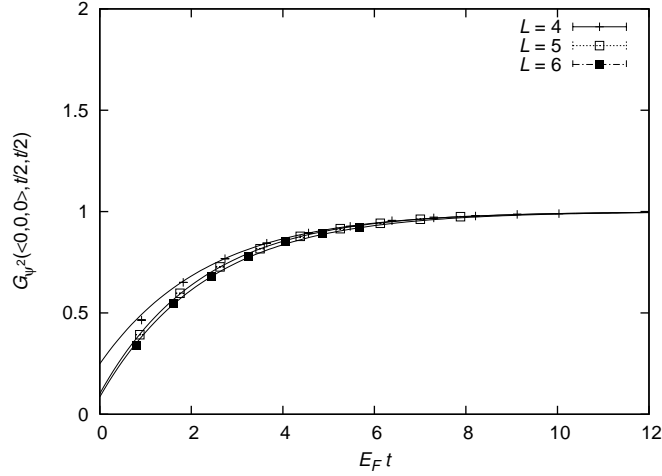


FIG . 3: A comparison of $G_2^{(0;0,0>,t/2,t/2)}$ and the asymptotic $1 - \frac{b}{e} e^{-E_F t}$ for the 9;9 system with $L = 4;5;6$:

In FIG . 3 we show a comparison of the renormalized correlation function

$$G_2^{(0;t=2;t=2)} = \frac{1}{-G_2^{\text{bare}}(0;t=2;t=2)} \quad (61)$$

and the asymptotic t

$$1 - \frac{b}{e} e^{-E_F t} \quad (62)$$

for the 9;9 system and $L = 4;5;6$. In the unitary limit we expect agreement for different values of L when plotted as functions of $E_F t$, and this appears to be the case.

The energy E characterizing the exponential decay of the transient signal in $G_2^{(0;t=2;t=2)}$ is similar to the energy E measured in the function $N_{;N}(t)$ described in [11]. This might perhaps be a threshold for a certain type of excitation or a maximum in the overlap of ρ_0^{free} with the spectral density projection operator. The answer is not clear. In the next section we find another excitation with the same quantum numbers but much lower energy. This suggests that our fit with only one exponential time constant may not be a reliable method to determine the higher excitation energy, and a multistate analysis should be used. The interpretation of the apparent energy scale E will require further study.

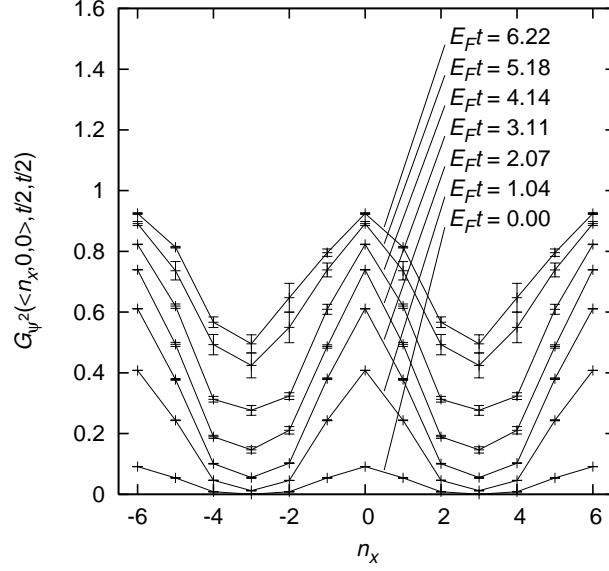


FIG . 4: The renormalized correlation function $G_2(\mathfrak{n}_s; t=2; t=2)$ for the 13;13 system with $L = 6$, $\mathfrak{n}_s = \ln_x; 0; 0i$, and $E_F t$ between 0 and 6.22.

IX . RESULTS FOR THE t-DEPENDENT PROFILE OF G_2

In all cases we consider systems with total momentum $\vec{P} = \vec{0}$ and total spin $S = 0$. In FIG . 4 we show the renormalized correlation function $G_2(\mathfrak{n}_s; t=2; t=2)$ for the 13;13 system at unitarity with $L = 6$, $\mathfrak{n}_s = \ln_x; 0; 0i$, and $E_F t$ between 0 and 6.22. In order to make the periodicity of the lattice visually clear we show two full lattice lengths.

There are several features in this plot which indicate some interesting physics. First of all G_2 appears to have long range order. With a total of 26 particles we cannot probe distances far beyond k_F^{-1} . But for large $E_F t$ we find that $G_2(\mathfrak{n}_s; t=2; t=2)$ averaged over the entire lattice is greater than 0.5. We recall $G_2(\mathfrak{n}_s; t=2; t=2)$ is normalized so that the peak value at $\mathfrak{n}_s = \vec{0}$ is 1 as $E_F t \rightarrow \infty$. The second point of interest is that for $\mathfrak{n}_s \neq \vec{0}$ the transient signal has a very long time constant. This long constant time is not apparent at $\mathfrak{n}_s = \vec{0}$. There the transient signal has a shorter time constant, $(\frac{E}{\hbar})^{-1}$ in the notation of the previous section. The slow transient signal corresponds with a much lower energy scale and appears to have an approximate $\cos(2\pi n_x/L)$ spatial dependence.

The time constant is easier to see if we plot $G_2(\mathfrak{n}_s; t=2; t=2)$ as a function of $E_F t$. In FIG . 5 we show the renormalized correlation function $G_2(\mathfrak{n}_s; t=2; t=2)$ versus $E_F t$ for the

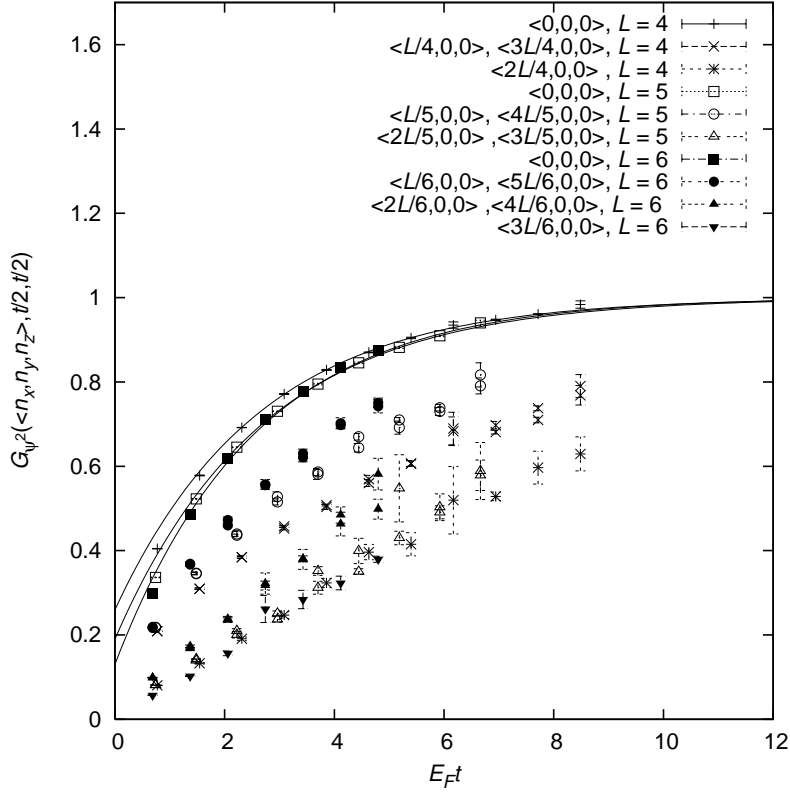


FIG . 5: The renormalized correlation function $G_2(\mathbf{n}_s; t=2; t=2)$ versus $E_F t$ for the 7;7 system with $L = 4;5;6$ and $\mathbf{n}_s = \langle n_x; 0; 0 \rangle$. For visual clarity datapoints with errorbars exceeding 0.1 are not shown.

7;7 system with $L = 4;5;6$ and $\mathbf{n}_s = \langle n_x; 0; 0 \rangle$. We can see quite clearly the fast exponential tail of the transient signal for $\mathbf{n}_s = \mathbf{0}$ and the slow exponential tail for $\mathbf{n}_s \neq \mathbf{0}$. In the unitary limit, $G_2(\mathbf{n}_s; t=2; t=2)$ as a function of $E_F t$ for different L should agree for the same ratio $\mathbf{n}_s=L$. The data in FIG . 5 shows quite clearly this unitary limit scaling.

In FIG . 6 the renormalized correlation function $G_2(\mathbf{n}_s; t=2; t=2)$ is shown for the 5;5 system with $L = 4;5;6$ and $\mathbf{n}_s = \langle n_x; 0; 0 \rangle$. We again see the fast exponential tail of the transient signal at $\mathbf{n}_s = \mathbf{0}$ and the slow exponential tail for $\mathbf{n}_s \neq \mathbf{0}$. There is good agreement for different values of L with the same $\mathbf{n}_s=L$.

In FIG . 7 $G_2(\mathbf{n}_s; t=2; t=2)$ is shown for the same 5;5 system with $L = 4;5;6$; but this time along the z-axis, $\mathbf{n}_s = \langle 0; 0; n_z \rangle$. In this case the long time constant previously seen for $\mathbf{n}_s \neq \mathbf{0}$ is no longer visible. The distinction between the x- and z-axes can be explained by the non-SO(3;Z) invariant momentum killing for $\frac{\text{free}}{0}$. As shown in Table 1, $\frac{\text{free}}{0}$ contains

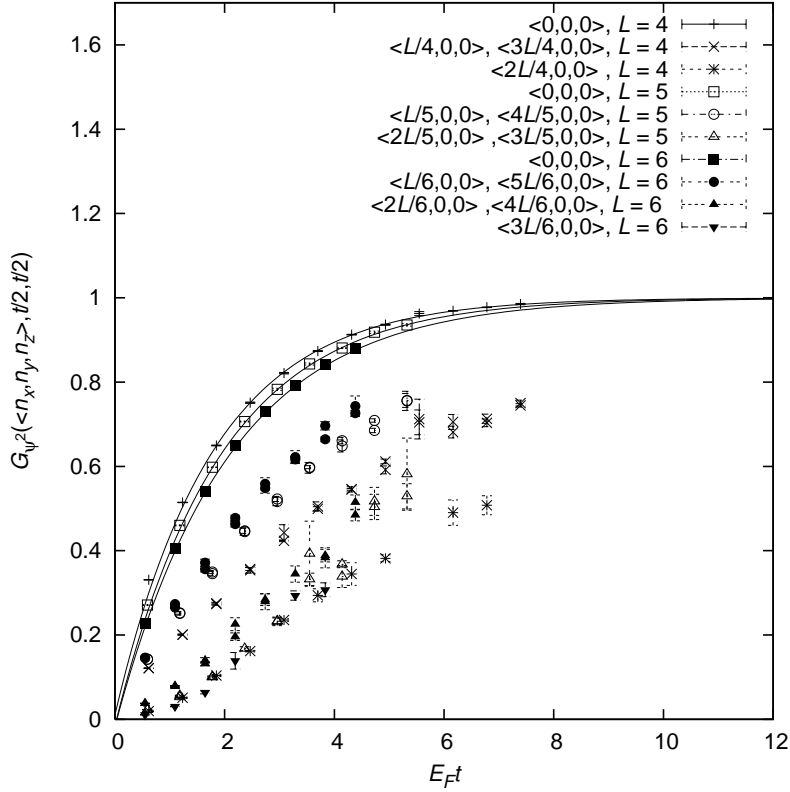


FIG .6: The renormalized correlation function $G_2(\mathbf{n}_s; t=2; t=2)$ versus $E_F t$ for the 5;5 system with $L = 4;5;6$ and $\mathbf{n}_s = n_x; 0; 0$. For visual clarity datapoints with errorbars exceeding 0:1 are not shown.

the momentum states $\frac{2}{L}; 0; 0$ and $\frac{2}{L}; 0; 0$ but not the momentum states $0; 0; \frac{2}{L}$ and $0; 0; \frac{2}{L}$. This produces an overlap with some low-energy excitation with an approximate $\cos(2 n_x=L) - 1$ profile in $G_2(\mathbf{n}_s; t=2; t=2)$ but a much weaker overlap if the same excitation is aligned along the z-axis. It would seem therefore that the excitation is some type of two-particle state with constituents moving in opposite directions with momentum $\frac{2}{L}$.

X. RESULTS FOR THE LOWEST EXCITATION ENERGY

We now measure the energy of the lowest excitation. We first construct combinations of $G_2(\mathbf{n}_s; t_1; t_2)$ which maximize the signal to noise ratio. For $N = 3$ the low-energy excitation does not couple strongly to $G_2(\mathbf{n}_s; t_1; t_2)$ for \mathbf{n}_s along the y- and z-axes. Therefore we use

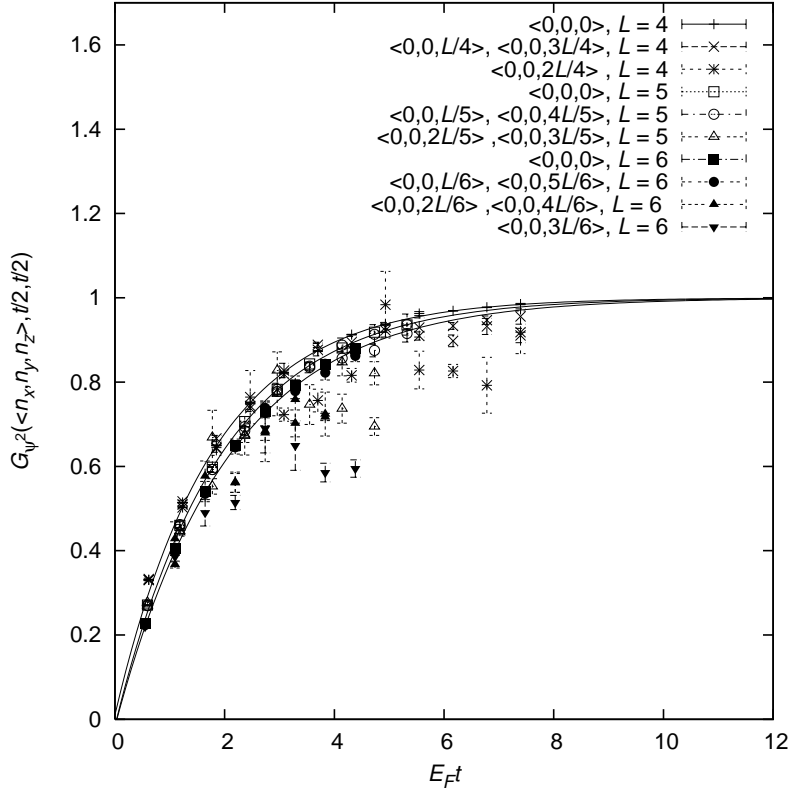


FIG .7: The renormalized correlation function $G_{xy}^2(\langle n_s; t=2; t=2 \rangle)$ versus $E_F t$ for the 5;5 system with $L = 4;5;6$ and $n_s = \langle 0;0;n_z \rangle$. For visual clarity datapoints with errorbars exceeding 0:1 are not shown.

only data along the x-axis. We define

$$\begin{aligned}
 & \frac{2}{x} G_{xy}^2(t_1; t_2) \\
 & = L^2 \left[G_{xy}^2(0; t_1; t_2) + \frac{1}{2} [G_{xy}^2(\langle n_1; 0; 0i; t_1; t_2 \rangle) + G_{xy}^2(\langle n_{-1}; 0; 0i; t_1; t_2 \rangle)] \right] : \quad (63)
 \end{aligned}$$

For $N = 5$ the coupling is weak only along the z-axis and so we define

$$\begin{aligned}
 & \frac{2}{xy} G_{xy}^2(t_1; t_2) \\
 & = L^2 \left[G_{xy}^2(0; t_1; t_2) + \frac{1}{4} [G_{xy}^2(\langle n_1; 0; 0i; t_1; t_2 \rangle) + G_{xy}^2(\langle n_{-1}; 0; 0i; t_1; t_2 \rangle) \right. \\
 & \quad \left. + G_{xy}^2(\langle n_0; 1; 0i; t_1; t_2 \rangle) + G_{xy}^2(\langle n_0; -1; 0i; t_1; t_2 \rangle) \right] : \quad (64)
 \end{aligned}$$

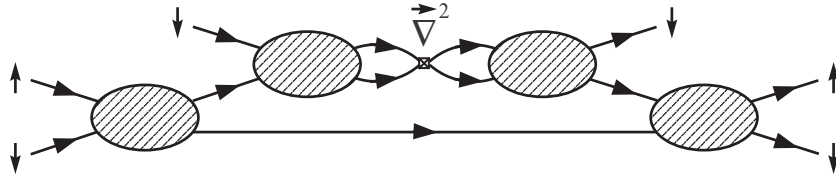


FIG .8: One insertion of the operator $\frac{1}{\tilde{r}^2} a_{\#}^y(\mathbf{x}) a_{\#}^y(\mathbf{x}) [a_{\#}(\mathbf{x}) a_{\#}(\mathbf{x})]$:

For $N = 7$ we define

$$\begin{aligned}
 & G_{xyz}^2(t_1; t_2) \\
 = & L^2 \int \int G^2(0; t_1; t_2) \left[\frac{1}{6} G^2(h1; 0; 0i; t_1; t_2) + G^2(h-1; 0; 0i; t_1; t_2) \right. \\
 & \left. + G^2(h0; 1; 0i; t_1; t_2) + G^2(h0; -1; 0i; t_1; t_2) \right. \\
 & \left. + G^2(h0; 0; 1i; t_1; t_2) + G^2(h0; 0; -1i; t_1; t_2) \right] : \quad (65)
 \end{aligned}$$

If no additional ultraviolet renormalization is required, then in the continuum limit we have

$$\frac{\partial_x^2 G^2(t_1; t_2)}{\partial_x^2 G^2(0; t_1; t_2)}; \quad (66)$$

$$\frac{\partial_{xy}^2 G^2(t_1; t_2)}{\partial_x^2 + \partial_y^2} G^2(0; t_1; t_2); \quad (67)$$

$$\frac{\partial_{xyz}^2 G^2(t_1; t_2)}{\partial_x^2 + \partial_y^2 + \partial_z^2} G^2(0; t_1; t_2); \quad (68)$$

To prove that no additional renormalization is needed it suffices to show that one insertion of the operator

$$\frac{1}{\tilde{r}^2} a_{\#}^y(\mathbf{x}) a_{\#}^y(\mathbf{x}) [a_{\#}(\mathbf{x}) a_{\#}(\mathbf{x})] \quad (69)$$

is finite. Just as we found for the insertion of $a_{\#}^y(\mathbf{x}) a_{\#}^y(\mathbf{x}) a_{\#}(\mathbf{x}) a_{\#}(\mathbf{x})$, the factor of \tilde{r}^{-2} takes care of the divergences from the two extra fermion bubbles. In the unitary limit the two-particle Green's function has the form

$$G^2(p_0; \mathbf{p}) / \frac{1}{m - m p_0 - \frac{\mathbf{p}^2}{4}}; \quad (70)$$

where p_0 is the total energy and \mathbf{p} is the total momentum of the two fermions. Consider now a diagram such as the one shown in FIG .8. Let p_0 be the energy and \mathbf{p} be the momentum of the internal loop. We cut the momentum at $|\mathbf{p}| = a^{-1}$ and cut the energy at $p_0 = m$.

If we now count powers of ϵ we get ϵ^5 from $\text{dp}_0 d^3 p$, ϵ^2 from the two Green's functions, ϵ^6 from the three fermion propagators, and ϵ^2 from the Θ^2 . The final result is ϵ^1 and so the integral is finite. In this way one can show that all diagrams involving one insertion of

$$-\frac{1}{\epsilon} a_{\#}^y(\mathbf{x}) a_{\#}^y(\mathbf{x}) \tilde{r}^2 [a_{\#}(\mathbf{x}) a_{\#}(\mathbf{x})] \quad (71)$$

are ultraviolet finite. This means that in the unitary limit each of the functions ${}^2_x G_2(t_1; t_2)$, ${}^2_{xy} G_2(t_1; t_2)$, ${}^2_{xyz} G_2(t_1; t_2)$ should be independent of L when considered as functions of $E_F t_1$ and $E_F t_2$.

In FIG. 9 we plot $\ln [{}^2_x G_2(t_1; t_2)]$ for the 3;3 system with $L = 4;5;6$. We have produced data for $t_1 = t_2$ and data for t_2 fixed at $E_F t_2 = 1.2$. The agreement for different values of L provides a consistency check of unitary limit scaling. In the continuum language we are calculating the logarithm of $\partial_x^2 G_2(0; t_1; t_2)$. Using the asymptotic expansion (11) we have

$$\begin{aligned} \partial_x^2 G_2(0; t_1; t_2) = & \partial_x^2 A_{00}(0) \partial_x^2 A_{01}(0) e^{(E_1 - E_0)t_2} \\ & \partial_x^2 A_{10}(0) e^{(E_1 - E_0)t_1} \partial_x^2 A_{11}(0) e^{(E_1 - E_0)(t_1 + t_2)} + \dots \quad (72) \end{aligned}$$

The fixed t_2 data as $t_1 \rightarrow 1$ is useful in extracting $E_1 - E_0$ since the time dependence must be proportional to $e^{(E_1 - E_0)t_1}$ plus a constant. We see from the plot that $\ln [{}^2_x G_2(t_1; t_2)]$ is nearly a straight line for large t_1 . This indicates a small asymptotic value at $t_1 = 1$, and a nearly pure exponential signal in this time window. We have fitted a straight line to determine the slope of $\ln [{}^2_x G_2(t_1; t_2)]$ with respect to $E_F t_1$ for the fixed t_2 data. We do the fit with a common slope for $L = 4;5;6$ but possibly different intercepts for the three values of L : While we are only fitting the fixed t_2 data, we see quite clearly the same slope appears in the $t_1 = t_2$ data.

In FIG. 10 we plot $\ln {}^2_{xy} G_2(t_1; t_2)$ for the 5;5 system with $L = 4;5;6$. We show data for $t_1 = t_2$ and t_2 fixed at $E_F t_2 = 1.6$: We do the same linear fits for the t_2 fixed data in order to extract $E_1 - E_0$. In FIG. 11 we plot $\ln {}^2_{xyz} G_2(t_1; t_2)$ for the 7;7 system with $L = 4;5;6$: In FIG. 12 we plot $\ln {}^2_{xyz} G_2(t_1; t_2)$ for the 9;9 system with $L = 4;5;6$: In FIG. 13 we plot $\ln {}^2_{xyz} G_2(t_1; t_2)$ for the 11;11 system with $L = 5;6$: In FIG. 14 we plot $\ln {}^2_{xyz} G_2(t_1; t_2)$ for the 13;13 system with $L = 5;6$:

In all cases we find agreement for different values of L as predicted by unitary limit scaling. In all cases we also find agreement between the slope of the fixed t_2 data and the

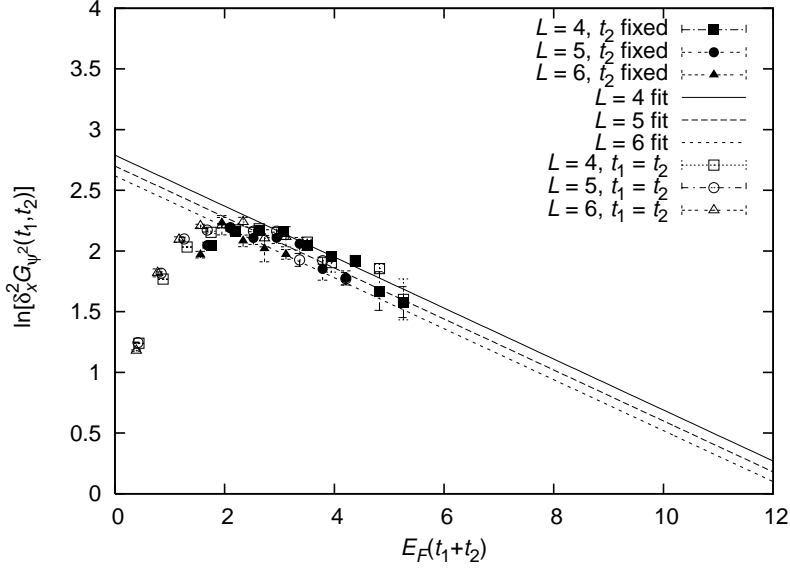


FIG . 9: Plot of $\ln G_x^2(t_1, t_2)$ for the 3;3 system with $L = 4;5;6$. We show data for $t_1 = t_2$ and t_2 fixed at $E_F t_2 = 12$.

$t_1 = t_2$ data when plotted as functions of $E_F(t_1 + t_2)$. This implies that the $e^{(E_1 - E_0)t_1}$ and $e^{(E_1 - E_0)t_2}$ terms are small so that

$$\tilde{r}^2 G_x^2(0; t_1; t_2) \approx \tilde{r}^2 A_{00}(0) + \tilde{r}^2 A_{11}(0) e^{(E_1 - E_0)(t_1 + t_2)}; \quad (73)$$

with \tilde{r}^2 replaced by ∂_x^2 for the 3;3 system and $\partial_x^2 + \partial_y^2$ for the 5;5 system :

We show the results for $E_1 - E_0$ in FIG . 15. We have plotted $(E_1 - E_0) = E_F$ versus momentum $k = k_F$ of the unknown constituents. This assumes that the excitation can be described as two constituents moving in opposite directions with momentum $\frac{2}{L}$. For comparison we show the linear part of the two-phonon dispersion relation at unitarity. We use the result [27]

$$c_s = \frac{r}{m} \frac{1}{3} \quad (74)$$

for the speed of sound and use the value $r = 0.25(3)$ reported in [1].

There are several things puzzling about this dispersion relation. The minimum in the energy occurs at about $0.8k_F$. Since this is close to k_F a reasonable interpretation is that the excitation consists of two fermionic quasiparticles. The problem though is that the energy $E_1 - E_0$ at $0.8k_F$ lies far below current estimates of 2ϵ , where ϵ is the even-odd staggering in the ground state energy. Fixed-node Green's function Monte Carlo simulations get a

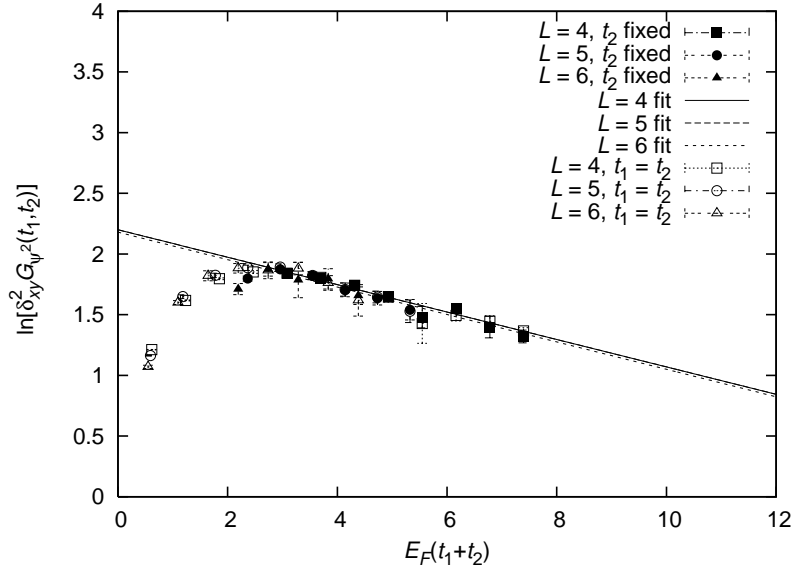


FIG. 10: Plot of $\ln G_{xy}^2(t_1, t_2)$ for the 5;5 system with $L = 4;5;6$. We show data for $t_1 = t_2$ and t_2 fixed at $E_F t_2 = 1.6$:

value $= 0.57(3)E_F$ for 12–20 particles in a periodic cube [28] and $= 0.50(3)E_F$ for 54–66 particles [29]. Our own lattice simulations for ω are in progress, but there is no evidence for ω being an order of magnitude lower than the fixed-node Monte Carlo results.

It is likely that our systems of 6–26 particles have too few particles to get an accurate reading for the excitation spectrum. Indeed there are not enough particles to probe the small $k=k_F$ behavior where the lowest excitations are described by phonons. Perhaps this low-energy excitation changes character and goes up in energy as we include more particles and long wavelength phonons emerge. This is possible. However we should still answer the question of what is happening in the 6–26 particle system and how it is able to produce an excitation this low in energy.

XI. PATH INTEGRAL PERMUTATIONS

Consider a path integral Monte Carlo calculation for identical noninteracting bosons from Euclidean time $t = 0$ to $t = \beta$; where β is the inverse temperature. During this time interval the individual boson worldlines undergo Brownian motion in three dimensions. From $t = 0$ to $t = \beta$ the average magnitude of the spatial displacement for each worldline is comparable

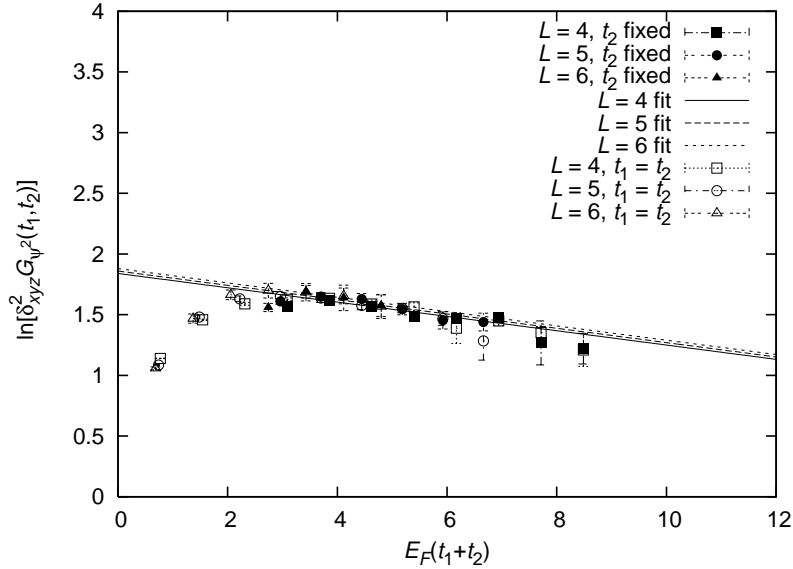


FIG .11: Plot of $\ln \delta_{xyz}^2 G_{\Psi}^2(t_1, t_2)$ for the 7×7 system with $L = 4, 5, 6$. We show data for $t_1 = t_2$ and t_2 fixed at $E_F t_2 = 2.0$:

to the thermal wavelength,

$$\tau = \frac{r}{\frac{2}{m}} \quad (75)$$

At nonzero temperature and sufficiently large systems, no individual worldline is able to explore the entire volume of the system. For classical distinguishable particles this is what would be required for each particle to relax into the zero momentum state. However Bose-Einstein condensation occurs when τ is about the same size as the interparticle spacing. The reason this is possible is because Bose symmetry allows for the permutation of identical particles as we go from $t = 0$ to $t = \tau$. As an example we show a permutation of four bosons in FIG .16. If the permutation of bosons with their neighbors results in the formation of macroscopic-scale permutation cycles, then we have the possibility of superfluid long range order [30]. This has been studied in path integral Monte Carlo calculations by measuring winding numbers around a periodic boundary [31].

We now consider what happens with identical fermions. A permutation cycle is a permutation which produces a ring exchange of a subset of elements

$$c : i_1 \rightarrow i_2; i_2 \rightarrow i_3; \dots; i_k \rightarrow i_1; i_{k+1} \rightarrow i_{k+2}; \dots; i_n \rightarrow i_{k+1} \quad (76)$$

A permutation cycle of identical fermions produces a plus sign if the cycle has an odd

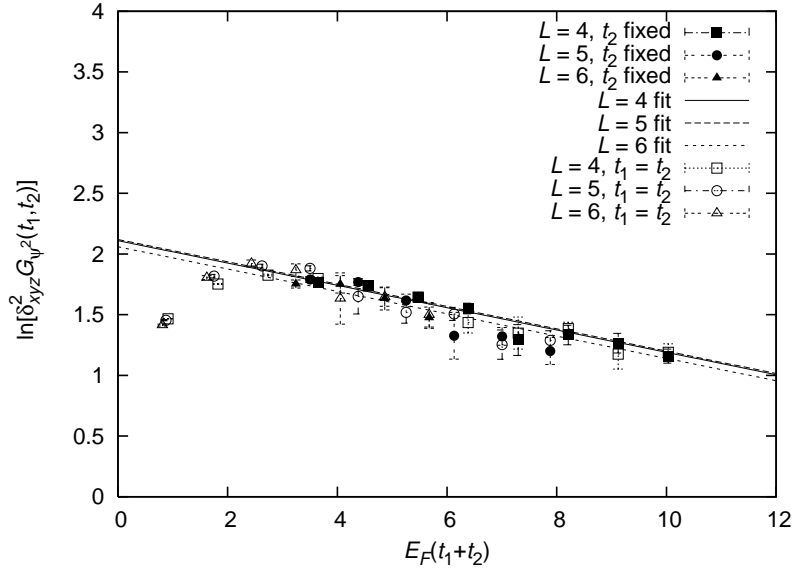


FIG. 12: Plot of $\ln |G_{xyz}^2(t_1, t_2)|$ for the $9;9$ system with $L = 4;5;6$. We show data for $t_1 = t_2$ and t_2 fixed at $E_F t_2 = 2.3$:

number of elements and a minus sign if the cycle has an even number of elements. Any permutation can be written as a product of disjoint permutation cycles. Therefore produces a minus sign if its disjoint cycle decomposition has an odd number of even length permutation cycles. Otherwise produces a plus sign. The interference between plus and minus sign permutations significantly reduce the total amplitude of the path integral. In computational quantum physics this cancellation is called the fermion sign problem and is one way to understand the higher energy for the ground state of Fermi systems when compared with Bose systems with the same interactions.

The representation of as a product of disjoint cycles is unique. However it is also useful to also view as a time sequence of permutation cycles. These cycles are not necessarily disjoint and so the product is noncommutative. We write the time sequence of cycles from right to left,

$$= G_M \dots C_3 C_2 C_1 : \quad (77)$$

c_1 occurs at the earliest time, then c_2 , and so on. While not unique, this gives a physical picture of how the worldlines tangle as Euclidean time goes from $t = 0$ to $t = \beta$.

We demonstrate one way to construct a time sequence of cycles. For bookkeeping purposes we label the particles as $1;2; \dots ;N$. Let the original positions be $1;2; \dots ;N$ at $t = 0$.

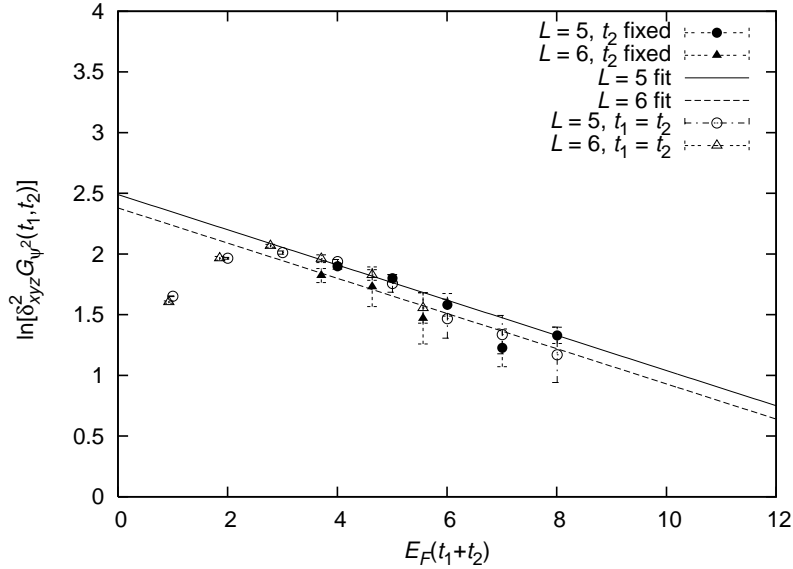


FIG .13: Plot of $\ln \delta_{xyz}^2 G_{\psi^2}(t_1, t_2)$ for the 11;11 system with $L = 5;6$. We show data for $t_1 = t_2$ and t_2 fixed at $E_F t_2 = 2:7$:

and divide the time interval into N_t steps of duration $\tau = \Delta t / N_t$. Let the positions of the particles after the j th time step be $\mathbf{r}_1^{(j)}; \mathbf{r}_2^{(j)}; \dots; \mathbf{r}_N^{(j)}$. Let $p^{(j)}$ be a permutation of the set $\{1; 2; \dots; N\}$ defined implicitly as the permutation which minimizes

$$\sum_{i=1; 2; \dots; N} \|\mathbf{r}_i^{(j)} - \mathbf{r}_{p^{(j)}(i)}^{(j-1)}\|^2 \quad (78)$$

In other words $p^{(j)}$ is a permutation of the particles from their original positions which best approximates their current locations after time step j . We note that $p^{(N_t)}$ equals p . We can now write p as a telescoping product

$$p = p^{(N_t)} (p^{(N_t-1)})^{-1} \dots p^{(3)} (p^{(2)})^{-1} \dots p^{(2)} (p^{(1)})^{-1} \dots p^{(1)} \quad (79)$$

Finally we decompose each permutation in square brackets as a product of disjoint cycles

$$p^{(1)} = c_1^{(1)} c_2^{(1)} \dots \quad (80)$$

$$p^{(2)} (p^{(1)})^{-1} = c_1^{(2)} c_2^{(2)} \dots \quad (81)$$

$$p^{(j)} (p^{(j-1)})^{-1} = c_1^{(j)} c_2^{(j)} \dots \quad (82)$$

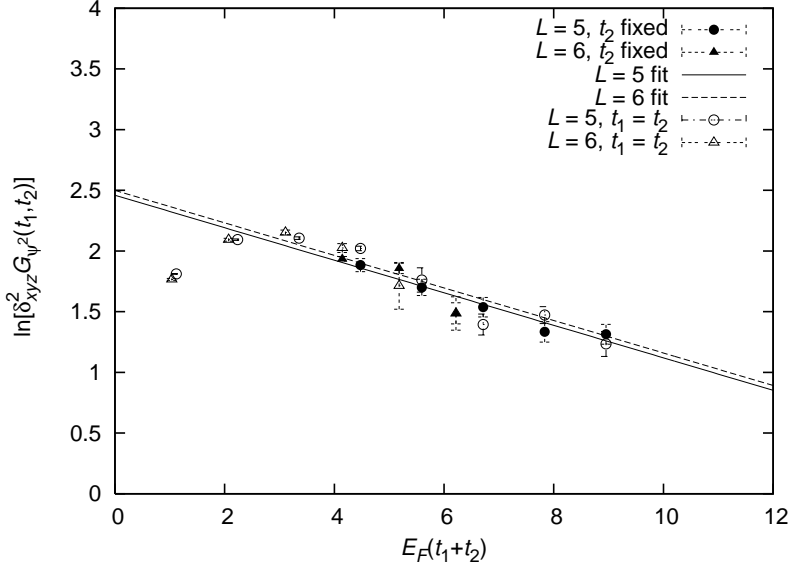


FIG .14: Plot of $\ln \delta_{xyz}^2 G_{\psi^2}(t_1, t_2)$ for the 13;13 system with $L = 5;6$. We show data for $t_1 = t_2$ and t_2 fixed at $E_F t_2 = 3.0$:

This gives us a time sequence of permutation cycles for time step t ,

$$= \begin{matrix} h & & i \\ c_1^{(N_t)} & c_2^{(N_t)} & \\ & & h \\ & & c_1^{(1)} & c_2^{(1)} & \\ & & & & i \end{matrix} : \quad (83)$$

We now consider in the path integral formalism spin-1/2 fermions with attractive interactions. Completely uncorrelated permutations for the up spins and down spins produce the same interference of plus and minus signs as for the free Fermi system. However if we take worldline configurations where the up and down spins undergo the same permutations then there are no minus signs at all. The contribution to the path integral from these permutations is a coherent sum of positive terms, just as in the case for identical bosons. In FIG .17 we show four identical up-spin fermions in black and four identical down-spin fermions in white. They undergo the same permutation, a clockwise 90 degree rotation when viewed from above.

This is the usual picture of strong fermionic pairing. The fermions form pairs and the pairs condense to form a superfluid. This is what happens in the strong-coupling BEC limit of spin-1/2 fermions. In that case the attraction is strong enough to produce tightly-bound dimers, and the two paired fermions move along their worldlines side-by-side.

This may not be the whole picture for the unitary limit. In the unitary limit the only physical scale is the average interparticle separation. Therefore superfluid pairs of fermions

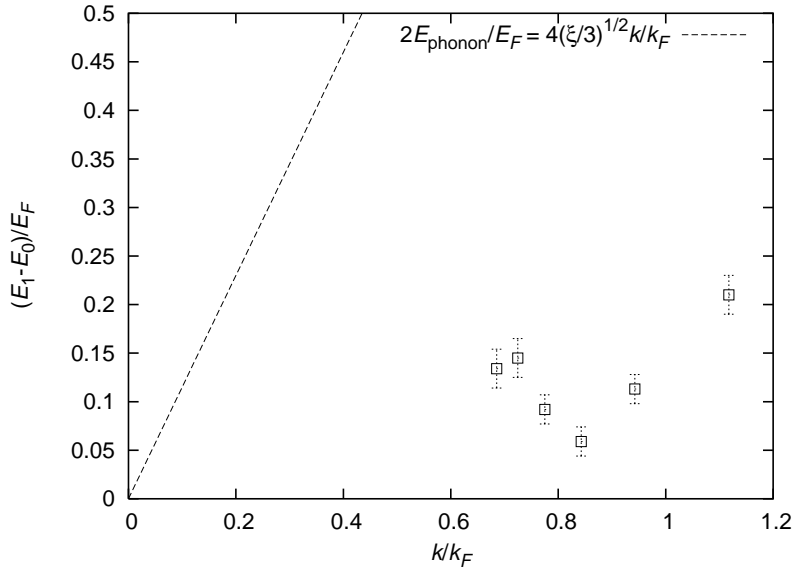


FIG . 15: Plot of $(E_1 - E_0)/E_F$ versus momentum k/k_F of the unknown constituents. For comparison we show the linear part of the two-phonon dispersion relation at unitarity.

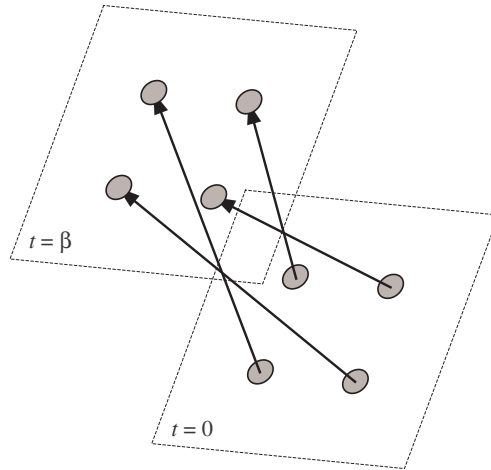


FIG . 16: Permutation of four identical bosons in the path integral formalism .

should be roughly the same size. We have just considered the case when paired up and down spins undergo the same permutation . We get a plus sign when we take into account Fermi statistics. However we also get a plus sign if the up spins are permuted by σ and the down spins are permuted by the inverse permutation σ^{-1} : In FIG . 18 we show four up spins permuting by a 90 degree clockwise rotation and four down spins permuting by a 90

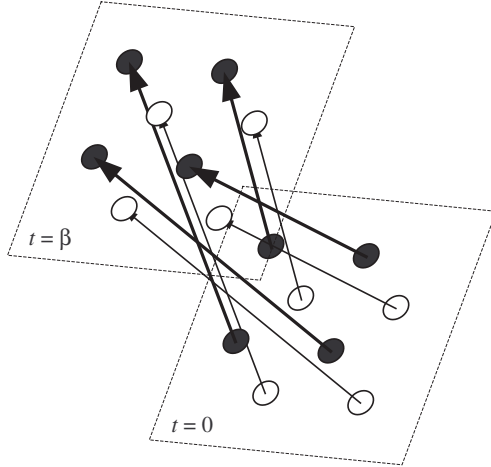


FIG .17: Four identical up-spin ferm ions are shown in black, and four identical down-spin ferm ions are shown in white. They undergo the same permutation, a clockwise 90 degree rotation when viewed from above.

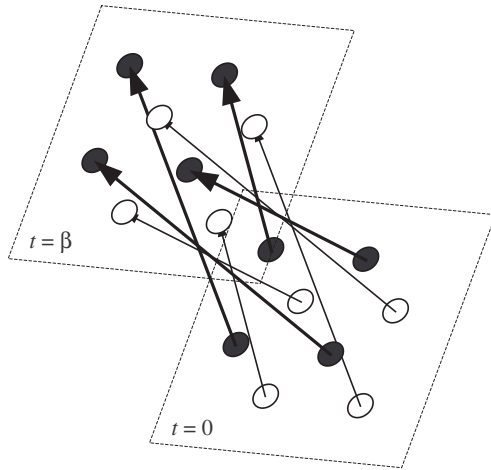


FIG .18: Four identical up-spin ferm ions are shown in black, and four identical down-spin ferm ions are shown in white. The up spins rotate clockwise 90 degrees while the down spins rotate counter-clockwise 90 degrees.

degree counterclockwise rotation.

This can be carried further. Let us decompose as a time sequence of permutation cycles

$$= \begin{matrix} \text{h} \\ c_1^{(N_t)} \end{matrix} \begin{matrix} \text{i} \\ c_2^{(N_t)} \end{matrix} \begin{matrix} \text{h} \\ c_1^{(1)} \end{matrix} \begin{matrix} \text{i} \\ c_2^{(1)} \end{matrix} : \quad (84)$$

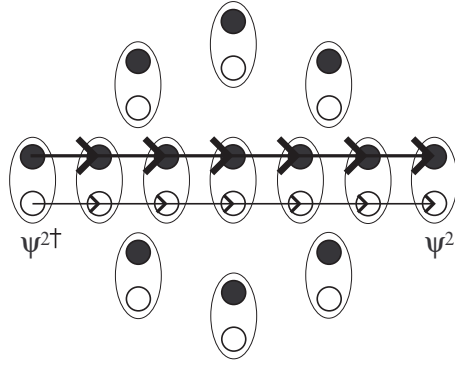


FIG .19: A line exchange of pairs producing a contribution to the ψ^2 correlation function

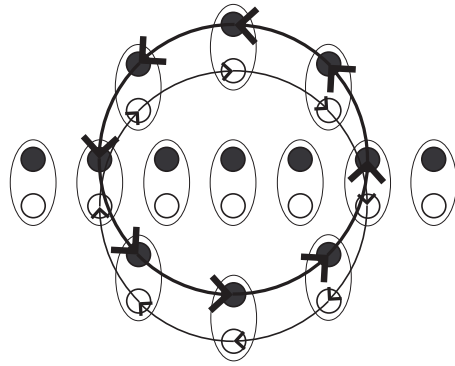


FIG .20: A countercycling permutation involving eight pairs in between the endpoints of the ψ^2 correlation function

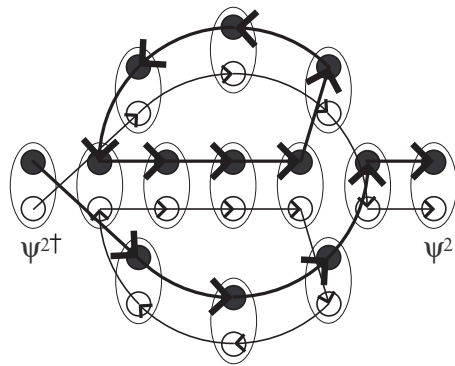


FIG .21: The result of implementing the countercycling permutation on the line exchange of pairs

based on the observed temperature dependence of the speed of second sound. Feynman gave a quantum-mechanical description of a roton as an excitation whose wavelength is resonant with the local spatial correlations of identical Bose particles [34, 35, 36]. He also derived an upper bound for the dispersion curve

$$E(k) = \frac{k^2}{2m S(k)}; \quad (87)$$

where $S(k)$ is the static structure factor. For ^4He a maximum in $S(k)$ occurs when $k = 2\pi/d$; where d is the average spacing between identical bosons. Therefore a minimum in the upper bound occurs at $k = 2\pi/d$, and this may also be reflected in $E(k)$. For very dilute Bose systems local spatial correlations are weaker and become significant only at distance scales comparable to the scattering length. In this case the maximum in $S(k)$ has been shown to occur at $k = 8\pi/a_{\text{scatt}}$ [37].

The particle density of superfluid ^4He at $T = 1.25\text{K}$ and $P = 1.0\text{atm}$ has been measured to be [38]

$$\frac{N}{V} = 2.20 \times 10^{22} \text{A}^{-3}; \quad (88)$$

Making a rough estimate for the average spacing

$$d = \left(\frac{N}{V}\right)^{-1/3}; \quad (89)$$

we get a theoretical prediction

$$k_R^{\text{theory}} = \frac{2\pi}{\left(\frac{N}{V}\right)^{-1/3}} = 1.76\text{A}^{-1}. \quad (90)$$

This compares quite well with a measurement of the roton minimum at $T = 1.26\text{K}$ and $P = 1.00\text{atm}$ [39];

$$k_R^{\text{exp}} = 1.902\text{A}^{-1}; \quad (91)$$

We can understand the role of Bose symmetry in determining k_R by considering a regular polygon of identical bosons. In FIG. 22 we show a regular polygon of identical particles with an odd number of vertices, and in FIG. 23 we show an even number of vertices. For bosons there will be no difference between odd and even. Let the angle between nearest-neighbor particles be θ and the corresponding arc length be d . A rigid rotation of the polygon by angle θ returns us to the same quantum state since it is a cyclical permutation of identical

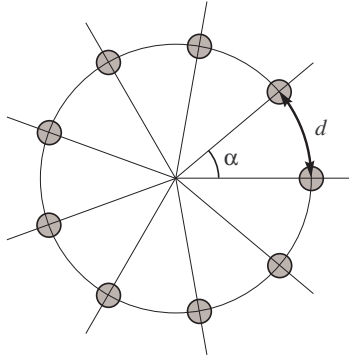


FIG .22: A regular polygon of identical particles with an odd number of vertices.

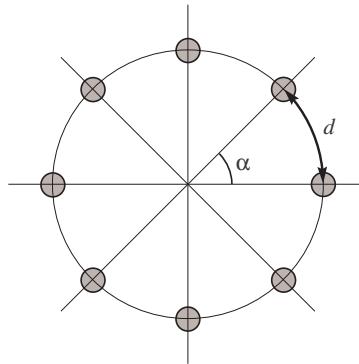


FIG .23: A regular polygon of identical particles with an even number of vertices.

Bose particles. If we allow the polygon to rotate about its center, then the total momentum k as measured along the circumference must satisfy

$$kd = 2\pi n \quad n = 0; 1; 2; \dots \quad (92)$$

The ground state occurs at $k = 0$ and the lowest nonzero momentum is at k_R , where $k_R = 2\pi/d$. Any momentum not a multiple of k_R requires exciting relative vibrational modes so that the quantum state must no longer transform as a singlet state under angle rotations.

We consider again the same system of regular polygons, but this time with identical fermions. We start with an odd number of vertices. A cyclical permutation of an odd number of identical fermions produces a plus sign under Fermi statistics. Therefore the allowed momenta for an odd 'train' of identical fermions is the same as that for identical

bosons,

$$k^{\text{odd}} = \frac{2}{d}n \quad n = 0; 1; 2; \dots \quad (93)$$

In contrast a cyclical permutation of an even number of identical fermions produces a minus sign under Fermi statistics. Therefore the allowed momenta for an even train of identical fermions is

$$k^{\text{even}} = \frac{\pi}{d} + \frac{2}{d}n \quad n = 0; 1; 2; \dots \quad (94)$$

If we were to consider evenly-spaced identical fermions in an antiperiodic box, then the formulas for k^{odd} and k^{even} would be reversed. In bulk macroscopic systems, boundary conditions should have little relevance to physical observables. So instead of distinguishing between odd and even numbers in a long train with many particles, it suffices to note that adding or removing one fermion changes the total momentum of the train by an amount πd plus some multiple of $2\pi d$.

This same momentum change occurs when adding or removing noninteracting fermions at zero temperature in one dimension. We put the system in a periodic box of length L . At zero temperature the momentum modes are filled in some sequence with increasing magnitude,

$$k = 0; \frac{2\pi}{L}; \frac{4\pi}{L}; \dots; \frac{2\pi}{L}n; \frac{2\pi}{L}n; \dots \quad (95)$$

If we have $2n$ fermions then the total momentum changes by $2\pi n = \pi L$ if we add or remove one fermion. Since the average interparticle spacing is $d = L/(2n)$, the momentum change is πd .

We now consider the ground state of spin-1/2 fermions in the unitary limit. We assume the size of the pairs to be comparable to the average interparticle spacing. We also assume some degree of local spatial correlation. We make a schematic drawing of a possible arrangement of pairs in a periodic box in FIG. 24. We have aligned the pairs so that the identical fermions form particle trains along the horizontal direction. In the top two rows we have trains with an odd number of particles in each. In the bottom two rows we have trains with an even number of particles in each. Since we have chosen a periodic box, the odd trains can have zero momentum without exciting relative vibrational modes while the smallest momentum each even train can have is πd . If the up and down spins in the bottom two rows move in the same direction, we have a roton excitation with momentum $2\pi d$. If however they move in opposite directions then the total momentum is zero.

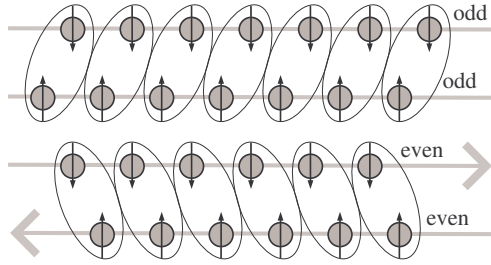


FIG . 24: Schem atic draw ing a possible arrangem ent of super uid pairs in a periodic box .

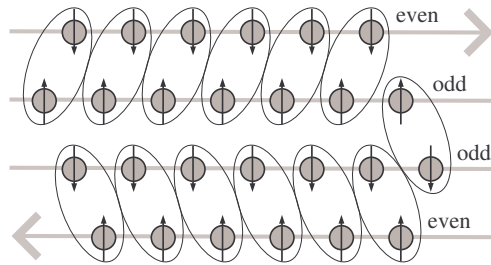


FIG . 25: Schem atic draw ing of a dislocation of the local spatial order of super uid pairs in a periodic box .

The relative velocity between the two rows implies that the pairing between these spins is not monogamous. However we can have pairing with interchanging partners produced by countercycling permutations of the type shown in FIG . 20.

Suppose now there is a dislocation in the local spatial order which changes the number of identical fermions in some of the particle trains. As an example we show in FIG . 25 the case when a pair originally in the top two rows realigns to sit in the second and third rows. In this case the even particle trains are located in the top and bottom rows. This produces a transverse separation of the $\pm d$ momenta. This momentum might be detected in the χ^2 correlation function and would have the signature of a two-particle state with constituents moving in opposite directions with momentum $\pm d$. For future reference we call this excitation a countermoving half-roton pair and define the half-roton momentum as

$$k_{R=2} = d: \tag{96}$$

If we make the same rough estimate for the average spacing,

$$d = \frac{N^{1/3}}{V} ; \quad (97)$$

then we get the prediction

$$k_{R=2} = \frac{1}{d} = \frac{1}{6} k_F^{1/3} = 0.306 k_F ; \quad (98)$$

This compares quite well with the lattice measurement of a minimum near $0.3k_F$.

XIII. DISCUSSION

The lattice data shows evidence for a low-energy two-particle excitation with constituents moving in opposite directions with momentum $0.3k_F$. The excitation is very low in energy and couples strongly to the χ^2 correlation function. This would seem to rule out a simple interpretation as two fermionic quasiparticles at energy 2ϵ . Instead we have given a possible interpretation of this excitation as a counter-moving half-roton pair within a framework of non-monogamous pairing. The counter-moving half-roton pair interpretation predicts a minimum at momentum $0.306k_F$. This is consistent with the lattice result.

A counter-moving half-roton pair looks similar to two fermionic quasiparticles. However the half-roton pair does not require breaking superfluid pairs since the pairing mechanism allows for the exchange of pair partners. This could explain the difference between the observed low excitation energy versus the larger energy 2ϵ . In the usual picture of monogamous pairing, counter-moving half-roton pairs do not exist. As the strength of the interaction is made stronger and we enter the BEC limit, pairing should become predominantly monogamous and the half-roton pair excitation energy would be comparable to 2ϵ .

While the location of the minimum at $k = 0.3k_F$ may be accurate as we go to macroscopic systems, the energy at the minimum may be significantly different in larger systems. The minimum energy measured at $k = 0.3k_F$ in these lattice simulations occurs in the 7×7 system, where $k_{R=2}$ corresponds with one wavelength wrapped around the lattice. This means that there are only two identical fermions in the particle train. In order to get a more accurate reading of the energy, we should have a minimum of four or more identical fermions in the particle train. Unfortunately this would mean a very large system with at least 120 particles or more. Further complicating matters is that a new computational problem would appear

when a two-phonon mode appears which is lower in energy. In that case maximum entropy methods or multistate techniques would be needed to see the higher energy signal.

The existence of a low-energy counterpropagating half-roton pair excitation would tend to drive down the superfluid critical temperature and create a pseudogap phase where single fermionic quasiparticles are gapped at ϵ_0 while counterpropagating half-roton pairs are gapped at a lower energy scale ϵ_0' . An estimate of the effect on the critical temperature requires a better understanding of ϵ_0' in large systems as well as the effective mass of the counterpropagating pair, the density of states, and possible interactions. It is possible though that this excitation could explain the consistently low critical temperature measured in recent lattice simulations which have looked for off-diagonal long-range order [17, 20, 40, 41].

For the polarized system it is possible that a single half-roton at momentum $k_{R=2} = 0.806k_F$ is a good description of the lowest-energy fermionic quasiparticle. Fixed-node Monte Carlo simulations have found a minimum at $k = 0.87k_F$ [29]. Lattice simulations for the $S = 1=2$ system are currently in progress. It is also possible that half-roton excitations could play a role in vortex lattices and vortex decays in polarized systems. At this stage the ideas are only speculative and much more work is needed to say whether or not non-monogamous pairing is realized in the unitary limit.

In order to make contact with recent observations of superfluidity with trapped ultracold atoms [42, 43, 44, 45, 46], we suggest that an emphasis be placed on universal observables in the unitary limit. These are observables that must agree in different physical systems at unitarity, such as critical temperature, critical velocity, speed of sound, low-energy excitation energies, etc. The reason for the emphasis on universal observables is that different microscopic theories can agree on all low-energy physical observables but disagree on wavefunctions and off-shell Green's functions. There has been some recent work on the non-universality of fermion momentum occupation numbers with respect to field redefinitions [47, 48]. By analogy similar issues have been raised concerning the universality of superfluid condensate fractions for a low-energy effective theory without specification of the fundamental microscopic physics.

XIV . S U M M A R Y

We have presented lattice results for spin-1/2 fermions at unitarity, where the effective range of the interaction is zero and the scattering length is infinite. We measured the spatial coherence of difermion pairs for a system of particles with equal numbers of up and down spins in a periodic cube. Using a transfer matrix projection method with auxiliary fields, we analyzed both ground state properties and transient behavior due to low-energy excitations. The results indicate a low-energy excitation consistent with two unknown constituents moving in opposite directions at approximately 0.8 times the Fermi momentum. However the excitation lies well below twice the pairing gap and couples strongly to the difermion order parameter. In order to explain this we developed a theoretical framework for non-monogamous pairing. We predict a lowering of the ground state energy by means of countercycling permutations of up-spin and down-spin fermions. If non-monogamous pairing is realized in the unitary limit, then it allows an interpretation of the low-energy excitation as a countermoving half-roton pair.

XV . A C K N O W L E D G E M E N T S

The author is grateful to Gautam Rupak and Thomas Schafer for many stimulating discussions. This work is supported in part by the DOE grant DE-FG 02-04ER 41335.

-
- [1] D.M. Eagles, *Phys. Rev.* 186, 456 (1969).
 - [2] A.J. Leggett, in *Modern Trends in the Theory of Condensed Matter. Proceedings of the XVth Karpacz Winter School of Theoretical Physics, Karpacz, Poland, 1980* (Springer-Verlag, Berlin, 1980), p.13.
 - [3] P.Nozières and S.Schmitt-Rink, *J. Low Temp. Phys.* 59, 195 (1985).
 - [4] Q.Chen, J.Stajić, S.Tan, and K.Levin, *Physics Reports* 412, 1 (2005).
 - [5] E.Tiesinga, B.J.Verhaar, and H.T.C.Stoof, *Phys. Rev. A* 47, 4114 (1993).
 - [6] W.C.Stwalley, *Phys. Rev. Lett.* 37, 1628 (1976).
 - [7] P.Courteille, R.S.Freeland, D.J.Heinzen, F.A.van Abeelen, and B.J.Verhaar, *Phys. Rev. Lett.* 81, 69 (1998).

- [8] S. Inouye, M. R. Andrews, J. Stenger, H.-J. Miesner, D. Stamper-Kurn, and W. Ketterle, *Nature* 392, 151 (1998).
- [9] C. J. Pethick and D. G. Ravenhall, *Ann. Rev. Nucl. Part. Sci.* 45, 429 (1995).
- [10] J. M. Lattimer and M. Prakash (2004), [astro-ph/0405262](#).
- [11] D. Lee, *Phys. Rev. B* 73, 115112 (2006), [cond-mat/0511332](#).
- [12] O. Penrose and L. Onsager, *Phys. Rev.* 104, 576 (1956).
- [13] L. P. Gor'kov, *Soviet Phys. JETP* 7, 505 (1958).
- [14] J.-W. Chen and D. B. Kaplan, *Phys. Rev. Lett.* 92, 257002 (2004), [hep-lat/0308016](#).
- [15] D. Lee and T. Schaefer, *Phys. Rev. C* 72, 024006 (2005), [nucl-th/0412002](#).
- [16] D. Lee, B. Borasoy, and T. Schaefer, *Phys. Rev. C* 70, 014007 (2004), [nucl-th/0402072](#).
- [17] M. W. Ingate (2005), [cond-mat/0502372](#).
- [18] A. Bulgac, J. E. D. Nutt, and P. Magierski, *Phys. Rev. Lett.* 96, 090404 (2006), [cond-mat/0505374](#).
- [19] D. Lee and T. Schaefer, *Phys. Rev. C* 73, 015201 (2006), [nucl-th/0509017](#).
- [20] D. Lee and T. Schaefer, *Phys. Rev. C* 73, 015202 (2006), [nucl-th/0509018](#).
- [21] M. Creutz, *Phys. Rev. D* 38, 1228 (1988).
- [22] M. Creutz, *Found. Phys.* 30, 487 (2000), [hep-lat/9905024](#).
- [23] B. Borasoy, H. Krebs, D. Lee, and U. G. Meissner, *Nucl. Phys. A* 768, 179 (2006), [nucl-th/0510047](#).
- [24] M. Luscher, *Commun. Math. Phys.* 105, 153 (1986).
- [25] S. R. Beane, P. F. Bedaque, A. Parreno, and M. J. Savage, *Phys. Lett. B* 585, 106 (2004), [hep-lat/0312004](#).
- [26] S. Duane, A. D. Kennedy, B. J. Pendleton, and D. Roweth, *Phys. Lett. B* 195, 216 (1987).
- [27] D. T. Son and M. W. Ingate, *Annals Phys.* 321, 197 (2006), [cond-mat/0509786](#).
- [28] S. Y. Chang, V. R. Pandharipande, J. Carlson, and K. E. Schmidt, *Phys. Rev. A* 70, 043602 (2004).
- [29] J. Carlson and S. Reddy, *Phys. Rev. Lett.* 95, 060401 (2005), [cond-mat/0503256](#).
- [30] R. P. Feynman, *Phys. Rev.* 91, 1291 (1953).
- [31] D. M. Ceperley, *Rev. Mod. Phys.* 67, 279 (1995).
- [32] L. D. Landau, *J. Phys.* 5, 71 (1941).
- [33] L. D. Landau, *J. Phys.* 11, 91 (1947).

- [34] R. P. Feynman, *Phys. Rev.* 91, 1301 (1953).
- [35] R. P. Feynman, *Phys. Rev.* 94, 262 (1954).
- [36] R. P. Feynman and M. Cohen, *Phys. Rev.* 102, 1189 (1956).
- [37] J. Steinhauer, R. Ozeri, N. Katz, and N. Davidson (2003), [cond-mat/0303375](#).
- [38] W. H. Keesom, *Helium* (Elsevier, Amsterdam, 1942).
- [39] O. W. Dietrich, E. H. Graf, C. H. Huang, and L. Passell, *Phys. Rev. A* 5, 1377 (1972).
- [40] E. Burovski, N. Prokofev, B. Svistunov, and M. Troyer, *Phys. Rev. Lett.* 96, 160402 (2006), [cond-mat/0602224](#).
- [41] E. Burovski, N. Prokofev, B. Svistunov, and M. Troyer (2006), [cond-mat/0605350](#).
- [42] C. A. Regal, M. Greiner, and D. S. Jin, *Phys. Rev. Lett.* 92, 040403 (2004).
- [43] J. Kinast, S. L. Hemmer, M. E. Gehm, A. Turlapov, and J. E. Thomas, *Phys. Rev. Lett.* 92, 150402 (2004).
- [44] M. W. Zwierlein, C. A. Stan, C. H. Schunck, S. M. F. Raupach, A. J. Kerman, and W. Ketterle, *Phys. Rev. Lett.* 92, 120403 (2004), [cond-mat/0403049](#).
- [45] M. Bartenstein, A. Altmeyer, S. Riedl, S. Jochim, C. Chin, J. Hecker Denschlag, and R. Grimm, *Phys. Rev. Lett.* 92, 120401 (2004).
- [46] M. W. Zwierlein, J. R. Abo-Shaeer, A. Schirotzek, C. H. Schunck, and W. Ketterle, *Nature* 435, 1047 (2005), [cond-mat/0505635](#).
- [47] R. J. Fumstahl, H. W. Hammer, and N. Trefessa, *Nucl. Phys. A* 689, 846 (2001), [nucl-th/0010078](#).
- [48] R. J. Fumstahl and H. W. Hammer, *Phys. Lett. B* 531, 203 (2002), [nucl-th/0108069](#).